PL-TR-94-2084
Environmental Research Papers, No. 1148

ASSESSMENT OF THE AN/FPS 118 IONOSPHERIC MODEL AND PROPOSED IMPROVEMENTS

B. S. Dandekar

1 March 1994

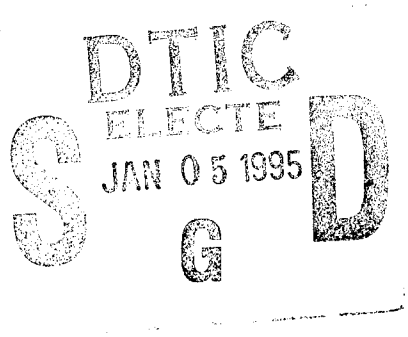

PHILLIPS LABORATORY
Directorate of Geophysics
AIR FORCE MATERIEL COMMAND
HANSCOM AIR FORCE BASE, MA 01731-3010

"This technical report has been reviewed and is approved for publication."

Maj Edward Berghorn, Chief
Ionospheric Application Branch

WILLIAM K. VICKERY, Director
Ionospheric Effects Division

This report has been reviewed by the ESC Public Affairs Office (PA) and is releasable to the National Technical Information Service (NTIS).

Qualified requestors may obtain additional copies from the Defense Technical Information Center (DTIC). All others should apply to the National Technical Information Service (NTIS).

If your address has changed, or if you wish to be removed from the mailing list, or if the addressee is no longer employed by your organization, please notify PL/TSI, 29 Randolph Road, Hanscom AFB, MA 01731-3010. This will assist us in maintaining a current mailing list.

Do not return copies of this report unless contractual obligations or notices on a specific document requires that it be returned.

REPORT DOCUMENTATION PAGE

Form Approved
OMB No. 0704-0188

1. AGENCY USE ONLY (Leave blank)	2. REPORT DATE	3. REPORT TYPE AND DATES COVERED
	1 March 1994	Scientific Interim

4. TITLE AND SUBTITLE
Assessment of the AN/FPS 118 Ionospheric Model and Proposed Improvements

5. FUNDING NUMBERS
PE: 62101F
Proj: 4643 TA GH
Work Unit: 01

6. AUTHOR(S)
B.S. Dandekar

7. PERFORMING ORGANIZATION NAME(S) AND ADDRESS(ES)
Phillips Laboratory (GPIA)
29 Randolph Road
Hanscom AFB, MA 01731-3010

8. PERFORMING ORGANIZATION REPORT NUMBER
PL-TR-94-2084
ERP, No. 1148

9. SPONSORING/MONITORING AGENCY NAME(S) AND ADDRESS(ES)

10. SPONSORING/MONITORING AGENCY REPORT NUMBER

11. SUPPLEMENTARY NOTES
This report will be of interest to the Air Weather Service and the OTH-B radar operators for prediction/specification of ionospheric models.

12a. DISTRIBUTION/AVAILABILITY STATEMENT
Approved for Public Release; Distribution Unlimited

12b. DISTRIBUTION CODE

13. ABSTRACT (Maximum 200 words)
The AN/FPS-118 analytical model for the Over the Horizon Backscatter (OTH-B) radar, developed by General Electric Company for the frequency management and the coordinate registration of the radar operation, was installed at the PL computer center and was tested for accuracy. The errors in the computer logic as well as in documentation were identified and appropriate corrections for improving the performance of the model were carried out and tested at PL; they are recommended for implementation at the radar sites in this report.

14. SUBJECT TERMS
Ionospheric model, Model for OTH-B radar, High latitude model

15. NUMBER OF PAGES
66

16. PRICE CODE

17. SECURITY CLASSIFICATION OF REPORT	18. SECURITY CLASSIFICATION OF THIS PAGE	19. SECURITY CLASSIFICATION OF ABSTRACT	20. LIMITATION OF ABSTRACT
Unclassified	Unclassified	Unclassifed	SAR

Contents

Illustrations

Tables

Acknowledgements

The author thanks Mr. Jurgen Buchau and Dr. Gary Sales for their invaluable comments and interest in the work. He thanks Mr. Maurice Shirley, University of Massachusetts, Lowell for the data analysis for the trough study and Capt. Gary Huffines, now at the Space Forecast Center, for his help in the trough analysis. He also thanks Mr. David Sannrud and Mr. Nelson Bonito, RADEX Corporation, for their efforts in installing the AN/FPS 118 Analytical Model at the PL computer facility and for their strong support of the model evaluation.

Assessment of the AN/FPS 118 Ionospheric Model and Proposed Improvements

1. INTRODUCTION

For the frequency management of the Over-the Horizon Backscatter (OTH-B) radar and for the target coordinate registration and propagation assessments, Millman et al.[1] developed the AN/FPS 118 - Analytical Model Specification henceforth referred to as the OTH ionospheric model. The model is used to generate ionospheric profiles and parameters at the grid points in 100 nautical-mile increments along the radial from the radar, covering the OTH coverage area. The coordinate registration scheme computes the virtual height traces (synthetic ionograms) at the midpoints of the selected ground ranges from the OTH ionospheric model. Superposing the transmission curve on the synthetic ionogram traces provides the reflection height tables for the respective frequencies. The derived virtual height traces are also used to predict operational frequencies, especially at times and in sectors where the backscatter ionograms do not provide clear signatures of the ground scatter.

(Received for Publication 1 March 1994)

[1] Millman, G.H., Bowser, C.A. and Swanson, R.W. (1988) An ionospheric model for HF sky wave backscatter radar, NATO-AGARD Symposium on Ionospheric Structure and Variability on A Global Scale and Interactions with Atmosphere, Magnetosphere, Munich, Federal Republic of Germany, *AGARD Conf. Proc.* **441**:pp. 43-1 to 43-15.

The OTH ionospheric model is an updated version of the AFGWC polar model(1982) developed by the U. S. Air Force Global Weather Central (AFGWC).[2] The model uses the ITS-78 ionospheric model of Jones et al.[3] as the starting point. The basic model is driven by an 'effective sunspot number SSN_{eff}' computed by AFGWC from the foF_2 data for the past five days from a network of 50 ionospheric stations. Assuming persistence as the best prediction available, the least squared deviation fit of the ionospheric model to the past five days' foF_2 averages for each hour, produces an effective sunspot number SSN_{eff}, which is used to predict the ionospheric state for the current day. Using the effective auroral oval parameters Q_E and Kp, the AWS superposes the auroral E and F layer enhancement and the midlatitude F layer trough electron density depletion on the ITS-78 model. The ionospheric parameters obtained by the automated Air Weather Service (AWS) Digital Ionospheric Sounding System (DISS) net are used for real-time updating of the model at the radar sites.

The OTH ionospheric model was tested and evaluated at the Phillips Laboratory (formerly called the Geophysics Laboratory) after an in-house capability to run the model and to display various model outputs was developed. The results of these tests along with necessary and/or beneficial modifications are presented below.

2. THE OTH IONOSPHERIC MODEL

The OTH ionospheric model implemented in the East Coast Radar System (ECRS) has been documented in an unpublished paper (private communication, Carl Bowser, GE, 1988). Millman, Bowser and Swanson (1988)[4] have published the model without the updating scheme as a NATO-AGARD symposium report[1] (Millman et al. 1988). Both reports and a computer program of the model are used for testing the concepts, consistency and the working accuracy of the OTH ionospheric model. A copy of the OTH ionospheric model computer program was provided to PL by GE and has been installed at the PL computer facility. At the radar site, the computer program runs in a real time operational mode. For analysis, the program was modified at PL to run in a batch mode for the purpose of testing the model at PL. It is now, for example, possible to provide diurnal variations of a selected set of ionospheric parameters at points of interest, to permit comparison with test data.

Modifications found necessary were made in one copy of the model, while an unmodified version is being maintained as a reference .

---

2 Air Force Global Weather Central (1982) *AFGWC Polar Ionospheric Model*, Air Force Weather Central, Program Listing, Feb. 1982.

3 Jones, W.B., Graham, R.P. and Leftin, M. (1969) *Advances in Ionospheric Mapping by Numerical Methods*, National Bureau of Standards U. S. Dept. of Commerce NBS Tech. Note 337, May (Reissued as ESSA Tech. Note ERL 107 ITS 75 May 1969).

4 Bowser, C., *AN/FPS 118 Analytical Model Specification, Preliminary Draft*, Contractor General Electric Company, private communication.

3. MODEL ANALYSIS

The analysis examined four major areas of the OTH ionospheric model: 1) the auroral E region enhancement, 2) the midlatitude trough region, 3) the updating of the OTH ionospheric model using observations from stations of the AWS Digital Ionospheric Sounding Systems (DISS) net, deployed in the vicinity and inside the coverage area of the East Coast OTH radar operation, and 4) the interpolation scheme used when data from two DISS stations are applied to update a common area.

3.1 Auroral E Layer

The auroral oval (Feldstein and Starkov 1967)[5], auroral E layer, and the F layer trough boundaries used in the OTH ionospheric model were shown in Figure 1 of the report by Millman et al. (1988). This figure is reproduced as Figure 1 in this report for convenience. Note that the auroral E layer bounded by ϕ_N (with the foE_a maximum located at ϕ_M) and ϕ_S covers only the equatorward half of the Feldstein-Starkov (1967) oval defined by ϕ_P and ϕ_E, with ϕ_C as the oval center line. For $Q \geq 3$, ϕ_M, ϕ_S, and ϕ_E coincide. When $Q < 3$, ϕ_M is 1° poleward of ϕ_E. The trough boundaries are shown by ϕ_{Nt}, ϕ_{Mt}, and ϕ_{St}. The location of the lowest trough density is 1.5° equatorward of the northern trough boundary ϕ_{Nt} and has no Kp dependence. The equations defining various boundaries have been added to Figure 1.

The auroral foE_a modeled by the OTH ionospheric model is shown in Figure 2 for 0000 Corrected Geomagnetic (CGM) Local Time (LT). The CGM latitude dependence of foE_a(MHz) is shown in the figure for various Q values. The horizontal lines show the width of the Feldstein-Starkov auroral oval. Based on the early work of Wagner[6] (1972), the OTH ionospheric model defines the auroral E layer contribution peaking at the equatorial edge of the oval. The contribution extends in a triangular shape, only up to the edge of the oval. There is no auroral E layer in the poleward region beyond the center of the oval. The auroral E layer affects the propagation situation of the East Coast OTH Radar System (ECRS) only for part of the night. The radar is > 400 km due south of the average night time southwest extent of the auroral E layer, which translates into ranges ≥ 800 km away from the radar in the direction of the northernmost sectors of segment 1. Therefore only low angle rays are likely to be propagated via an auroral mode. However, the auroral E layer is an important source of ionospheric spread clutter to the ECRS.

---

5 Feldstein, Y.I. and Starkov, G.V. (1967) Dynamics of auroral belt and polar magnetic disturbances, *Planet. Space Sci.* **15**:209-229.

6 Wagner, R.A. (1972) *Modeling the Auroral E-layer in Arctic Ionospheric Modeling.* Five related papers by Gassman, G.E., Buchau, J., Wagner, R.A., Pike, C.A. and Hurwitz, M.G., Air Force Surveys in Geophysics, No. 241, AFCRL-72-0305, AD748796.

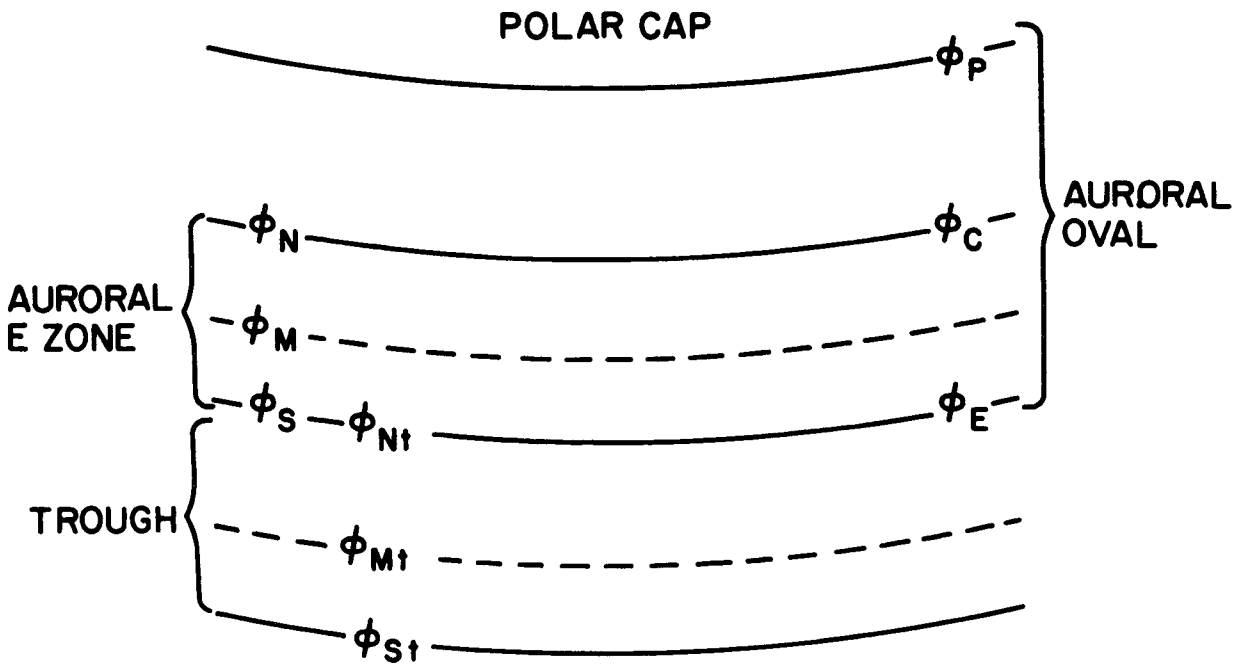

$$\phi_N = \phi_C = \frac{1}{2}(\phi_E + \phi_P) \quad \text{.....(5)}$$

$$\phi_M = \phi_E, \ \phi \geq 3 \quad \text{.....(9)}$$

$$\phi_M = \phi_E + 1°, \ \phi < 3 \quad \text{.....(10)}$$

$$\phi_{Nt} = \phi_E \quad \text{.....(34)}$$

$$\phi_{Mt} = \phi_E - 1.5° \quad \text{.....(43)}$$

$$\phi_{St} = \phi_E - 1.5 \text{ for } T_I \geq 0 \quad \text{.....(50)}$$

$$\phi_{St} = \phi_E + (3.7 + 1.3\ K_p)(.5 - \sqrt{R}) \text{ for } T_I < 0 \text{ and } R > 0.25 \quad \text{.....(48)}$$

$$\phi_{St} = \phi_E - 1.5 \text{ for } T_I < 0 \text{ and } R \leq 0.25 \quad \text{.....(49)}$$

Figure 1. Geomagnetic Orientation of the High Latitude Ionosphere.

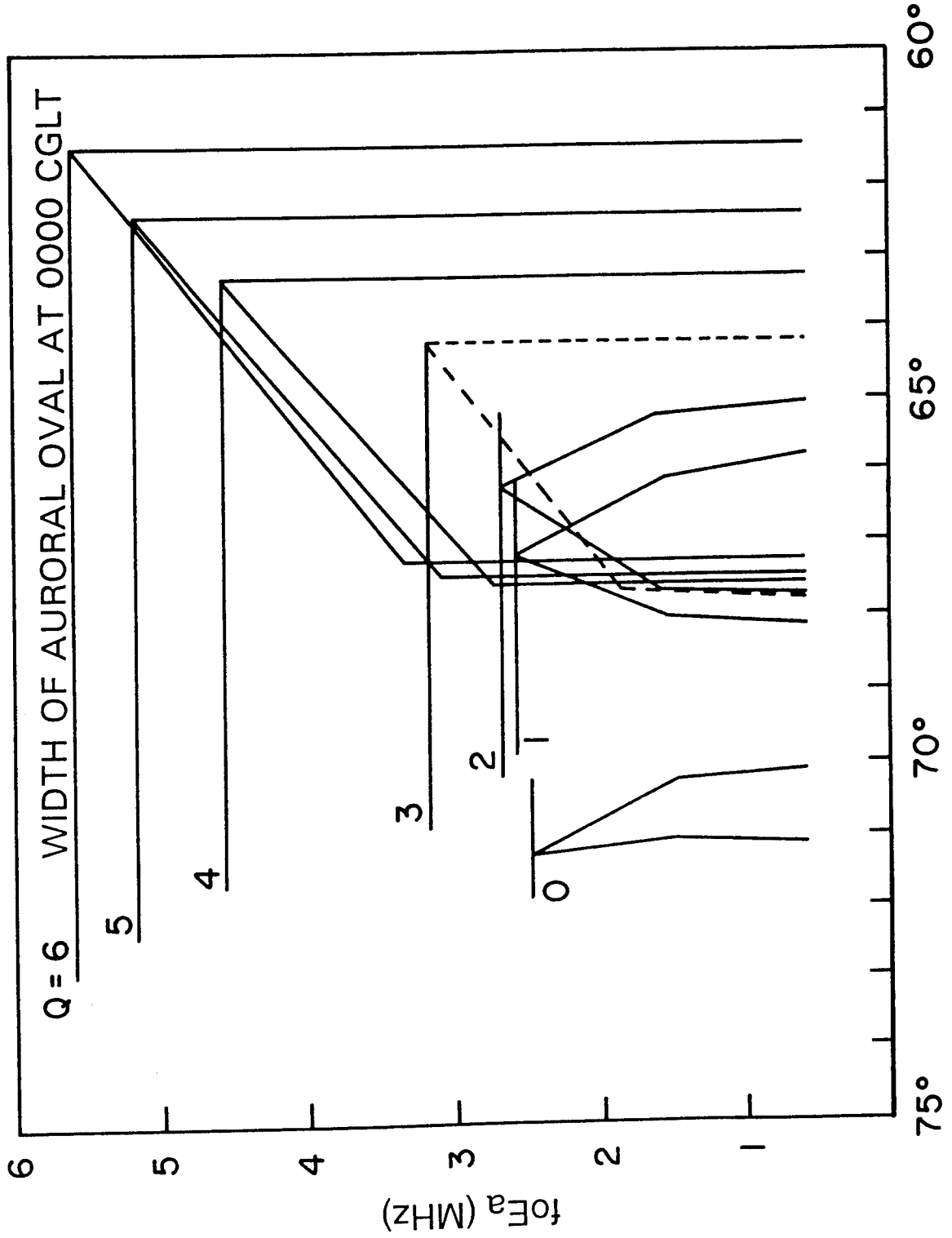

Figure 2. Latitudinal Dependence of foE_a for Various Q Values From the GE Model.

Reviewing the latitudinal distribution of the auroral E maximum electron density, Whalen[7] (1983), and Whalen et al.[8] (1985) have shown that statistically the auroral E layer peaks at the center of the Feldstein-Starkov oval and the auroral precipitation flux tapers off to the edges of the oval, following a Gaussian distribution. Using these recent results, Eqs. (5), (9), and (10) in Millman et al. (1988) have to be replaced by the following set:

$$\phi_N = \phi_P \text{ for Eq. (5)} \tag{1}$$

$$\phi_M = \phi_C \text{ for Eqs. (9) and (10)} \tag{2}$$

$$\phi_S = \phi_E \text{ (retained from Eq. (1) of Millman et al. (1988))} \tag{3}$$

where the L.H.S. refers to the foE_a boundaries and the R.H.S. refers to the Starkov[9] (1969) oval boundaries. In the OTH model the latitudinal distribution of foE_a is given by Eqs. (12) and (13):

$$foE_a = 0.6*(foE_a)_M + 0.4*(foE_a)_M\ (\phi_{MS} - \phi_M)/(\phi_M - \phi_S) \quad \text{Eq. (12) Millman et al. (1988)}$$

$$foE_a = 0.6*(foE_a)_M + 0.4*(foE_a)_M\ (\phi_{MN} - \phi_M)/(\phi_N - \phi_M) \quad \text{Eq. (13) Millman et al. (1988)}$$

Using Whalen's (1983) results, these two equations are replaced by a single equation:

$$foE_a = (foE_a)_M \exp\left(-3.*\left(\left((\phi_M - \phi)/(\phi_N - \phi_M)\right)^2\right)/2\right)^{1/4} \tag{4}$$

The results from these modifications are shown in Figure 3. Note that now the peak auroral foE_a is at the center of the oval and drops off symmetrically to the oval edges

---

7 Whalen, J.A. (1983) A quantitative description of the spatial distribution and dynamics of the energy flux in the continuous aurora, *J. Geophys. Res.*, **88A9**:7155-69.

8 Whalen, J.A. O'Neil, R.R. and Picard, R.H. (1985) The Aurora, in *Handbook of Geophysics and the Space Environment*, Air Force Geophysics Laboratory, AFGL-TR-85-0315, ADA16700.

9 Starkov, G.V. (1969) Analytical representation of the equatorial boundary of the auroral oval zone, *Geomag. and Aeronomy (Eng. Ed)*, **9**:614.

according to the fourth root of a Gaussian distribution. The latitudinal distribution of precipitating particle flux is a Gaussian. The fourth root enters the equation because the relation between the incident particle flux and the auroral foE_a is given by

$$\text{Flux} \propto (foE_a)^{1/4} . \tag{5}$$

Note that in Figures 2 and 3 the auroral foE_a curve for Q=0 is separate from the family of curves for other Q values. This happens because in the OTH model for Q=0, the Feldstein-Starkov[5] oval for Q is used, whereas for the remaining Q values Starkov's (1969) empirical equation is used. As a result the oval moves 4° equatorward from Q=0 to Q=1 and at a rate of one degree in latitude for each additional increment of $\Delta Q=1$ from Q=1 to Q=9.

The auroral E layer from the OTH ionospheric model and the proposed changes are shown in Figures 4 and 5 for Q=3, and in Figures 6 and 7 for Q=6. In the figures each block presents the Corrected Geomagnetic Local Time (CGMLT) marked at the left-hand top corner. The vertical lines show the foE_a boundaries. The comparison shows that the present OTH ionospheric model uses only 1/2 of the auroral oval width, and the auroral E distribution peaks at the equatorward boundary instead of at the center as in the improved Whalen (1983) model. The proposed changes are important to the radar coverage when the radar will actually be close to or under the auroral E region, as it will be in Alaska.

3.2 Midlatitude F Layer Trough

Current understanding of the behavior of the night time trough suggests a region of reduced electron density to the south of the equatorward boundary of the oval, extending from ~1 hour after sunset to the sunrise, when sunlight covering the polar cap provides a source of ionization, filling the trough region by antisunward convection. The OTH ionospheric model does not properly reproduce this.

(In his recent work, Whalen (1987, 1989)[10,11] has shown the existence of the trough wall into the daytime ionosphere along the equatorward boundary of the afternoon oval. This portion of the trough has been appropriately named the "daytime trough". The extent towards noon is strongly controlled by the magnetic activity. Due to its more northerly location than the post sunset trough, it is not relevant to the ECRS and has not been included in the current considerations. However, since it may be a source of daytime ionospheric clutter for the ECRS, and it may be of substantial importance to the ARS (Alaska Radar System), we will investigate its importance to the OTH radars at a later date.)

---

[10] Whalen, J.A. (1987) The daytime F layer trough observed on a macroscopic scale, *J. Geophys. Res.*, **92**:2571.

[11] Whalen, J.A. (1989) The daytime F layer trough and its relation to ionospheric – magnetospheric convection, *J. Geophys. Res.*, **94**:17169.

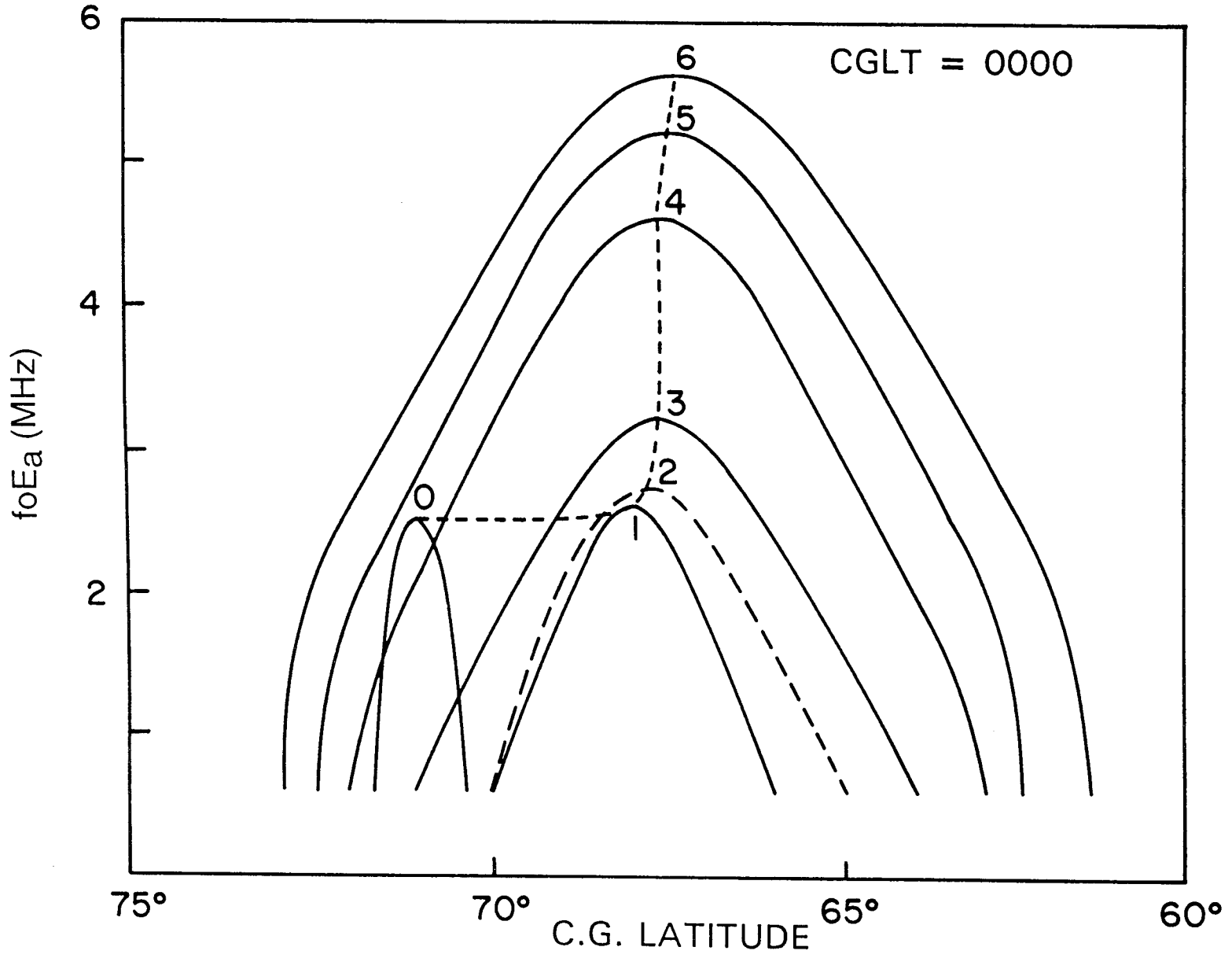

Figure 3. Latitudinal Dependence of foE_a for Various Q Values Using a Gaussian Distribution or the Incident Particle Flux.

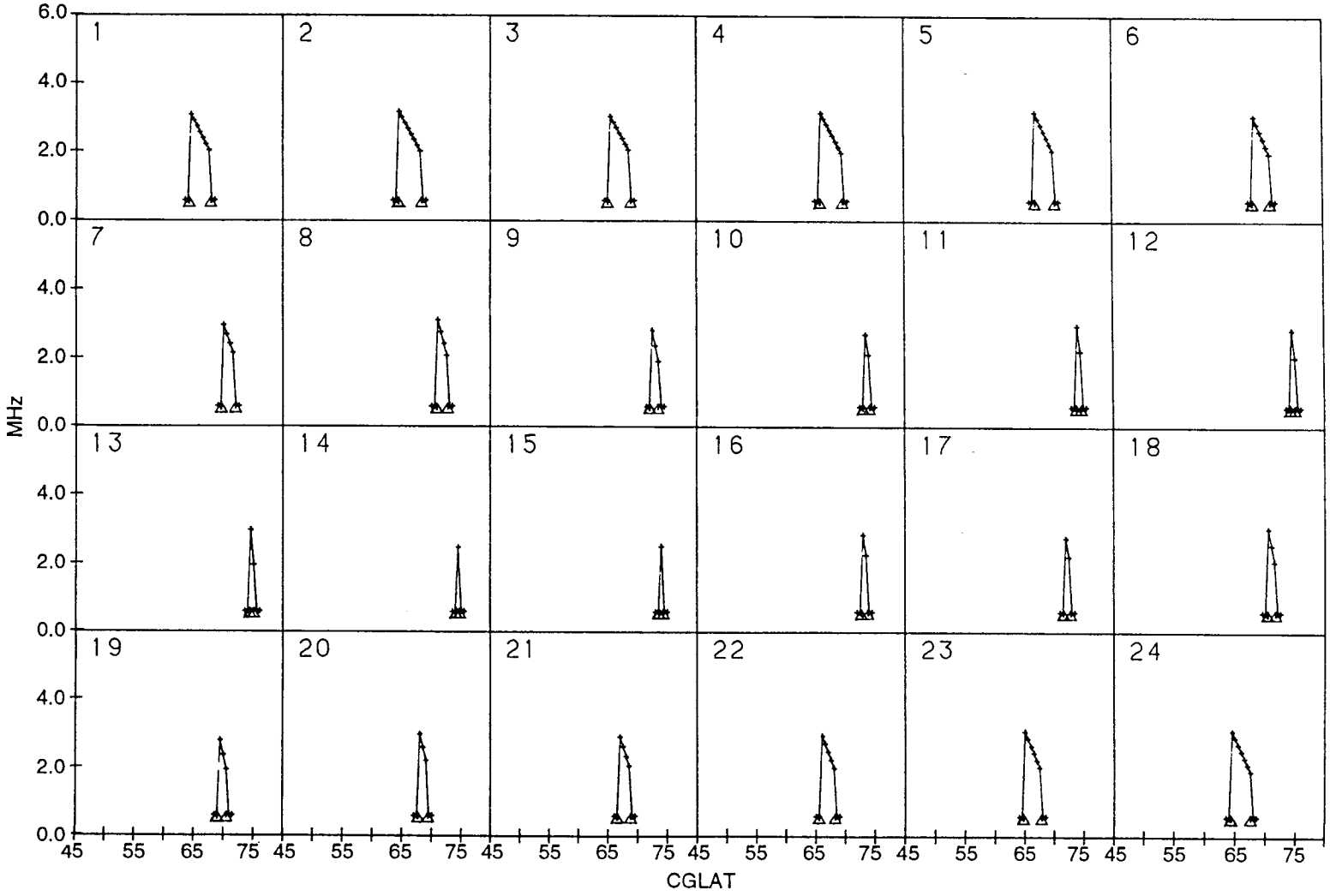

Figure 4. Latitudinal Distribution for Various CGT Hours for Q=3 From the GE Model.

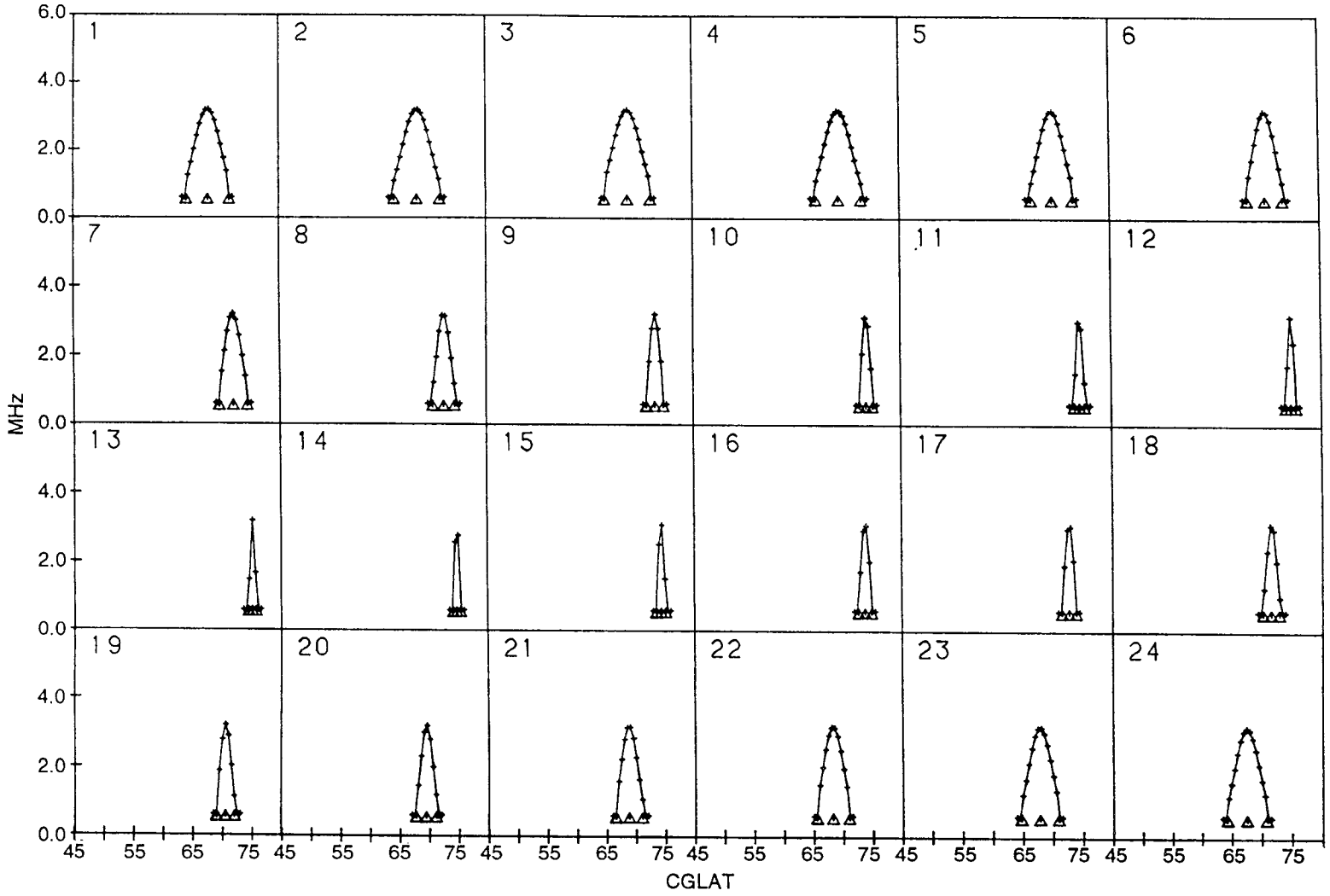

Figure 5. Latitudinal Distribution for Various CGT Hours for Q=3 Using a Gaussian Distribution for the Incident Particle Flux.

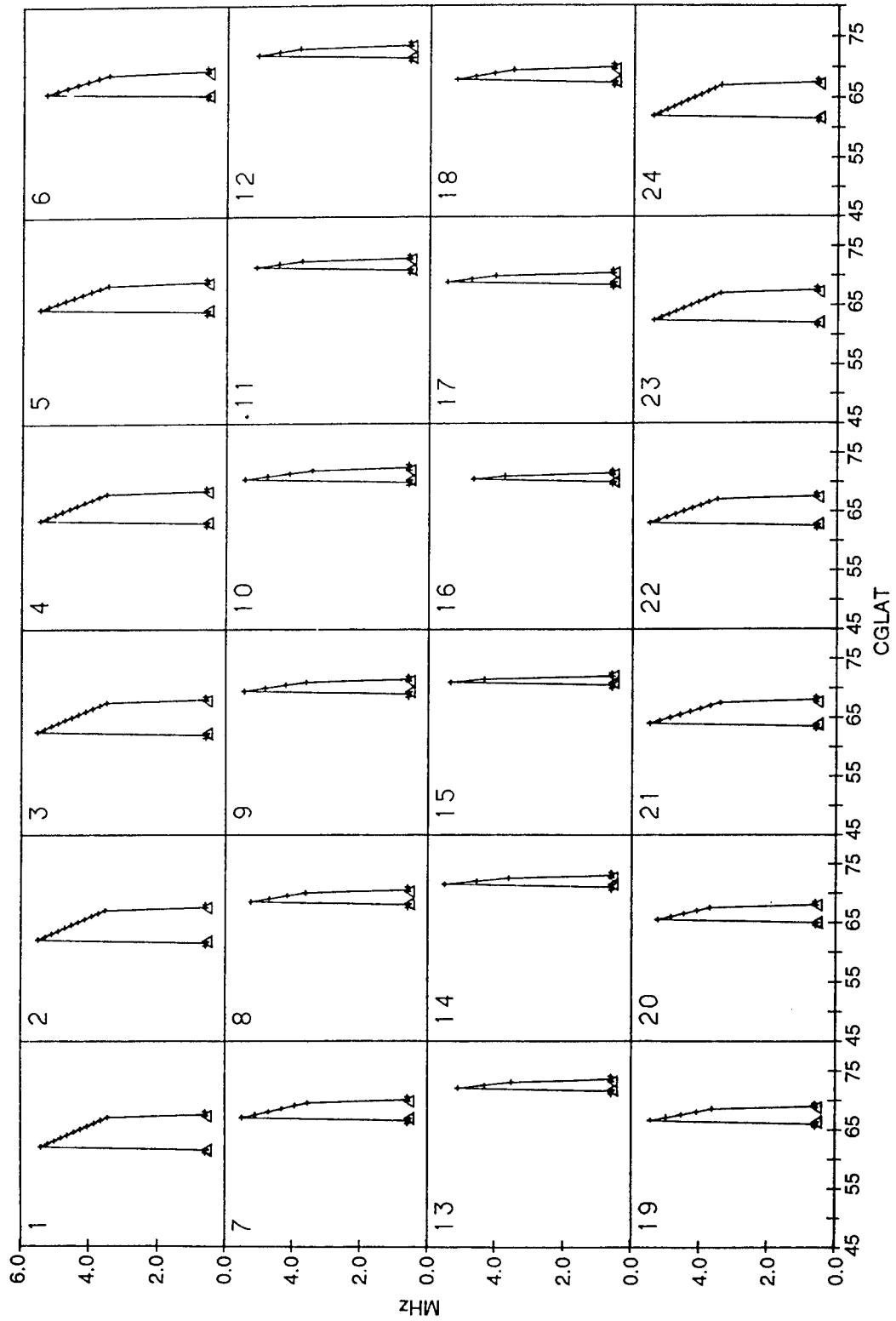

Figure 6. Latitudinal Distribution for Various CGT Hours for Q=6 From the GE Model.

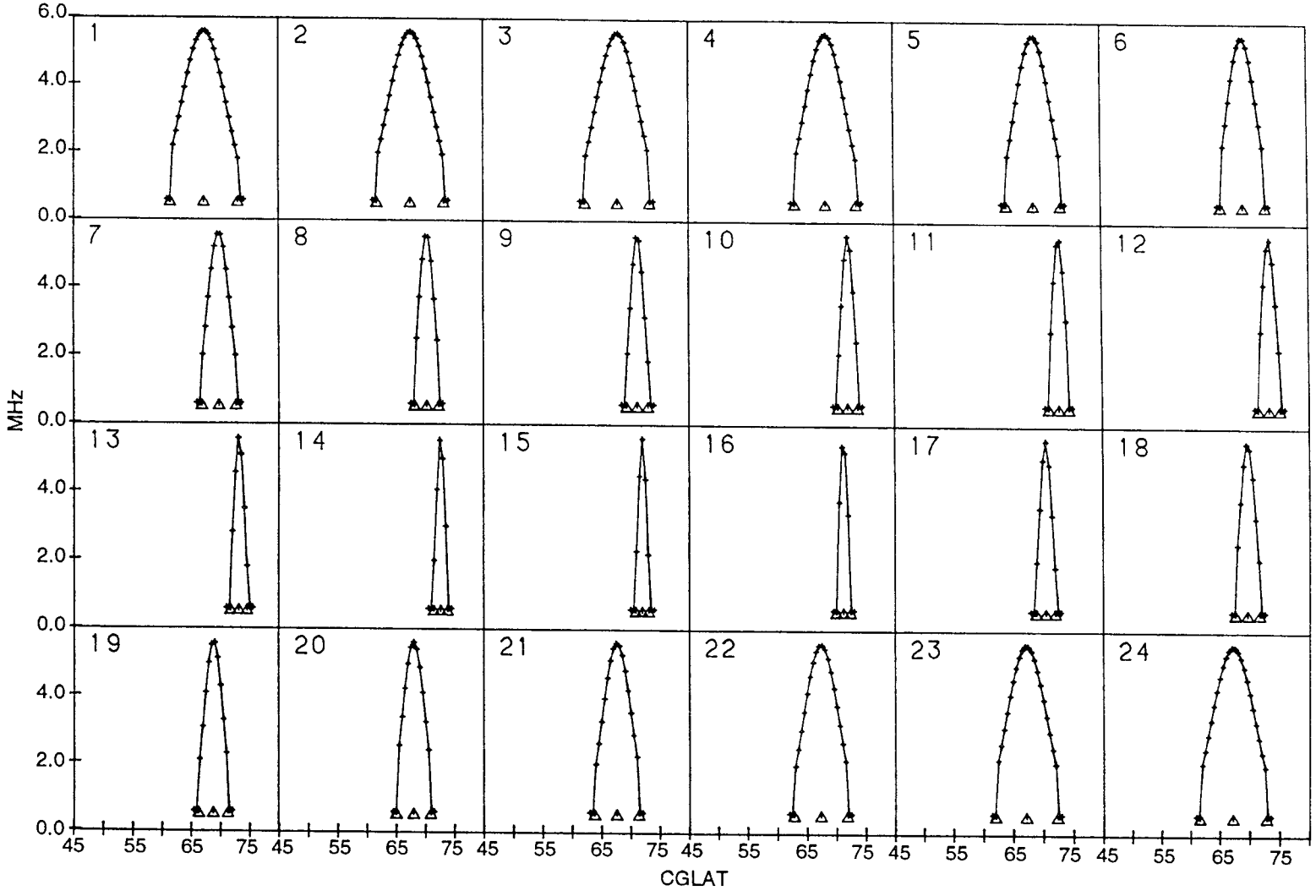

Figure 7. Latitudinal Distribution for Various CGT Hours for Q=6 Using a Gaussian Distribution for the Incident Particle Flux.

The correct definition of the trough is of importance to the ECRS, since the trough at night can extend deep into segment 1. The trough plays an even more important role in defining the propagation situation for the ARS, where it covers a large part of the ARS segment 10 ionospheric reflection region for 18 hours of each day (moderate conditions). The ARS segment 9 will be affected by the trough for approximately 6 hours each night. The equations defining the midlatitude F layer trough in the OTH ionospheric model, which are of concern in the present discussion, are listed below.

$$\Delta N = \tau\{1+\cos [2\pi (D+11)/365]\}$$ Eq. (36) Millman et al. (1988)

$$\tau = \tau_1 \exp [(X_1 - X_1^2)/2] \exp \{[- (t-3)^2]/12\}$$ Eq. (37) Millman et al. (1988)

$$X_1 = (\phi - \phi_E)/X_A$$ Eq. (38) Millman et al. (1988)

$$X_A = 3.7 + 1.3\ Kp$$ Eq. (39) Millman et al. (1988)

$$\tau_1 = -0.2$$ Eq. (41) Millman et al. (1988)

$$(h_mF_2)_{Mt} = 450\text{-}100\ V$$ Eq. (44) Millman et al. (1988)

$$R = 0.25 - [(t-3)^2/6] + 2 \log_e (-10\ \tau_1) +$$ Eq. (51) Millman et al. (1988)

$$2 \log_e \{1 + \cos [2\pi (D+11)/365]\}$$

The midlatitude F layer trough computed from the OTH ionospheric model is shown for Q=3 and Q=6 in Figures 8 and 9 respectively for Julian Day 354. In the figures each block presents the dependence of the trough reduction factor of foF_2 with CGM latitude for the CGMLT shown in the left hand top corner. The equatorward boundary (ϕ_{St}), deepest point (ϕ_{Mt}) and poleward boundary (ϕ_{Nt}) of the trough are marked by triangles. In the OTH model, the trough, as a night-time phenomenon, is correctly absent for 0700-1700 CGMLT. The figures however show that:

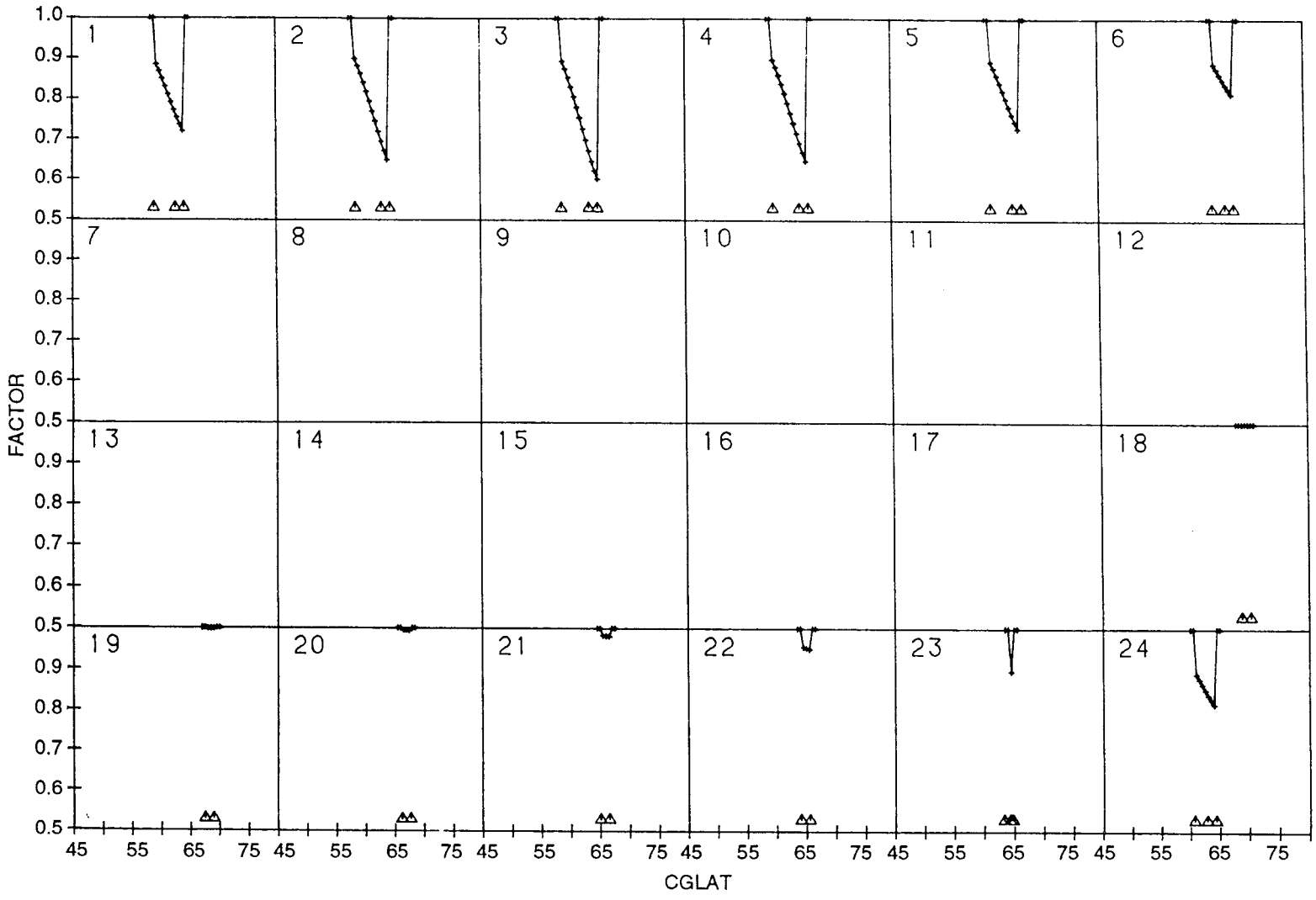

Figure 8. Latitudinal Distribution of the Trough Depletion Factor (1+n) for Various CGT Hours for Q=3 (Kp=1) From GE Model.

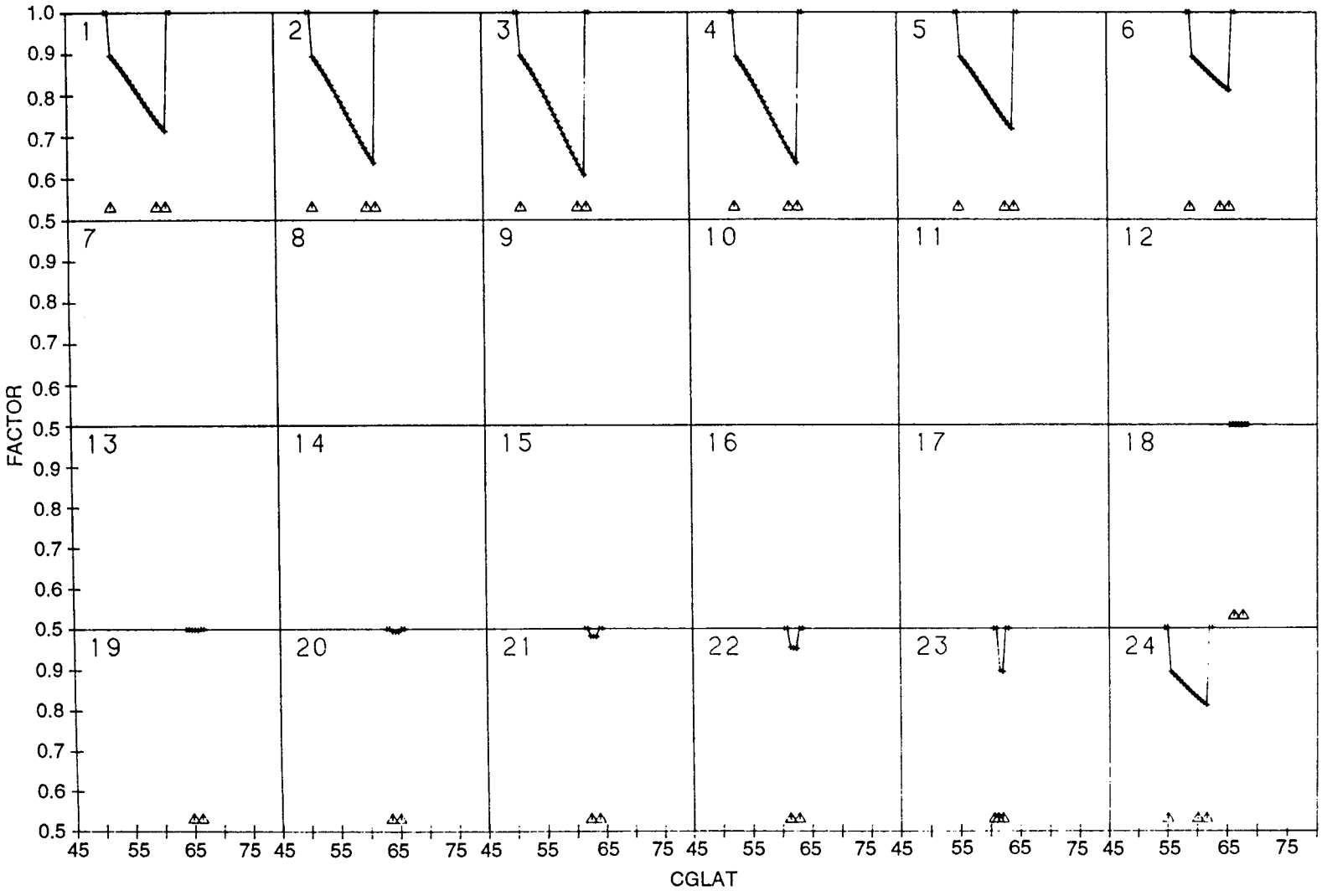

Figure 9. Latitudinal Distribution of the Trough Depletion Factor (1+n) for Various CGT Hours for Q=6 (Kp=4) From GE Model.

1) The modeled trough is very weak or absent up to 2300 CGMLT. This results from the vanishing of τ (Eq. (37), Millman et al. 1988) for $1800 \leq t \leq 2200$ CGMLT. Satellite observations (Halcrow and Nisbet 1977)[12] show that the trough is formed about 1 1/2 hrs after sunset. Goose Bay ionospheric soundings also show the onset of the trough after sunset for low magnetic activity. At Goose Bay the onset time moves to pre-sunset time as the magnetic activity increases (Buchau 1990, private communication). Recent aircraft measurements and resulting trough maps support this. These results are presented in Section 3.3.

2) The modeled trough has a sharp knife edge with no relation between the lowest value of the modifying factor and the latitude ϕ_{Mt} (see Figure 1). The location of the lowest point of the trough can be found by differentiating the latitude dependence term $\exp(-(X_1-X_1^2)/2)$ in Eq. (37) of Millman et al, which yields the value $X_1 = 0.5$. Substituting from Eq. (39) in Millman et al, we have

$$\phi_{Mt} = 0.5X_A + \phi_E = .5\,(3.7+1.3\ \mathrm{Kp}) + \phi_E \qquad (6)$$

Thus ϕ_{Mt}, the contour of the lowest electron density, in the trough lies equatorward of ϕ_E, the equatorward boundary of the auroral oval (same as the northward boundary of the trough) by 1.85 + 0.65 Kp degrees of latitude. This combined with the definition of ϕ_{Mt} ($=\phi_E$) produces a northern vertical wall of the trough.

3) The lowest trough critical frequency, is 0.6 foF_2. This corresponds to a reduction of 0.36 in electron density ($\propto foF_2^{2)}$ in the trough region. Satellite observations[12] show a reduction to 0.25 in the electron density (or a factor of 0.5 in foF_2) in the trough region.

4) A look at Eq. (36) (Millman et al. 1988) shows that the trough is absent in summer (Julian day (JD) 170) and deepest in winter (JD 354). When we increase the Julian Day in steps of 10 days the first occurrence of the trough is seen on JD 220. Thus the trough is absent from JD 170 -(220-170) to JD 220, that is, the trough is absent for (50*2=) 100 days, or more than 3 months. This likely underestimates the occurrence of the trough in summer and can be readily adjusted. We are currently analyzing Goose bay data to improve the occurrence statistics.

---

[12] Halcrow, B.W. and Nisbet, J.S. (1977) A Model of F_2 Peak Electron Densities in the Main Trough Region of the Ionosphere, *Radio Science*, **12**:815-820.

5) Figures 8 and 9 show a reduction of the trough width at 2300 hours. To understand this reduction in width, the CGMLT dependence of the trough width is determined from Eqs. (34) and (48)-(50) (Millman et al. 1988), and is shown in Figure 10. For 1800-2200 CGMLT the trough has a fixed width of 1.5° (and an insignificant depth as seen in Figures 8 and 9). From 2300-0600 CGMLT the trough width shows a systematic time dependence, provided by Eq. (48) (Millman et al. 1988). Equation (48) (Millman et al. 1988) which defines ϕ_{St} and Eq. (51) (Millman et al. 1988) which defines R, provide a time dependent width for 2300 to 0600 CGMLT. At 2300 CGMLT this width is smaller than 1.5°, used for prior hours. Equation (49) (Millman et al. 1988) assigns the width to the trough, but does not control the depth of the trough. The resulting width of the trough for 1800-2200 CGMLT shown in Figure 10 has no meaning since in this time sector the depth factor is zero or close to zero (see also discussion in 1) above).

To overcome the problems listed above the following changes are proposed:

a) The absence of the trough for 100 days can be reduced to 60 days by using the square root of the term $\{1+\cos[2\pi(D+11)/365]\}$ in place of the linear term.

b) The trough's deepest point is aligned with ϕ_{Mt} by replacing the $(X_1-X_1^2)/2$ term by $-X_1^2/2$ term.

c) As the trough is known to have a steeper foF_2 gradient (Pike 1976) on the poleward side than on the equator side, we define the range of the poleward wall as 1/5 the width of the trough. Therefore we have

$$\phi_{Mt} = \phi_{Nt} - (1/5)(\phi_{Nt} - \phi_{St}) \tag{7}$$

The shape of the trough is defined using the following equations:

$$\tau = \tau_1 \exp(-X_1^2/2) \exp[-(t-3)^2/12] \tag{8}$$

where X_1 is defined by the equation

$$X_1 = 2(\phi - \phi_{Mt})/X_A \quad (9)$$

and X_1 is replaced by $2X_1$ for $\phi > \phi_{Mt}$ resulting in a steeper foF_2 gradient for the poleward trough wall than the equatorward trough wall.

d) To generate the trough for the 1800-0000 CGMLT period, the t-3 term is set to zero for this interval. This produces a trough with constant depth and width for the 1800-0000 CGMLT interval.

e) Since the maximum depth of the trough is estimated to be 0.5 of the non-trough foF_2, τ_1 is adjusted from -1/5 to -1/3

$$\tau_1 = -1/3. \quad (10)$$

The trough resulting from the proposed modification is shown in Figures 11 and 12 for Kp=3 and 6 respectively. The figures show that: a) the trough is now present at night for 1800-0600 hours (CGMLT), b) the trough depth varies from 20 percent of unmodified foF_2 at 1800 CGMLT to approximately 50 percent at 0300 CGMLT, and recovers to 20 percent at 0600 CGMLT (sunrise), and c) the trough has poleward and equatorward walls; with the poleward wall steeper than the equatorward wall, supporting the observational evidence.

Equation (44) (Millman et al. 1988) fixes the trough height at an altitude 450 km at 0300 CGMLT with smooth lowering to 350 km at the terminators. The trough altitude is estimated to be 50 km above the ambient non-trough height. Therefore we propose the trough altitude as the height from the ITS-78 model +50 km, which ties the height of the trough to the background model height.

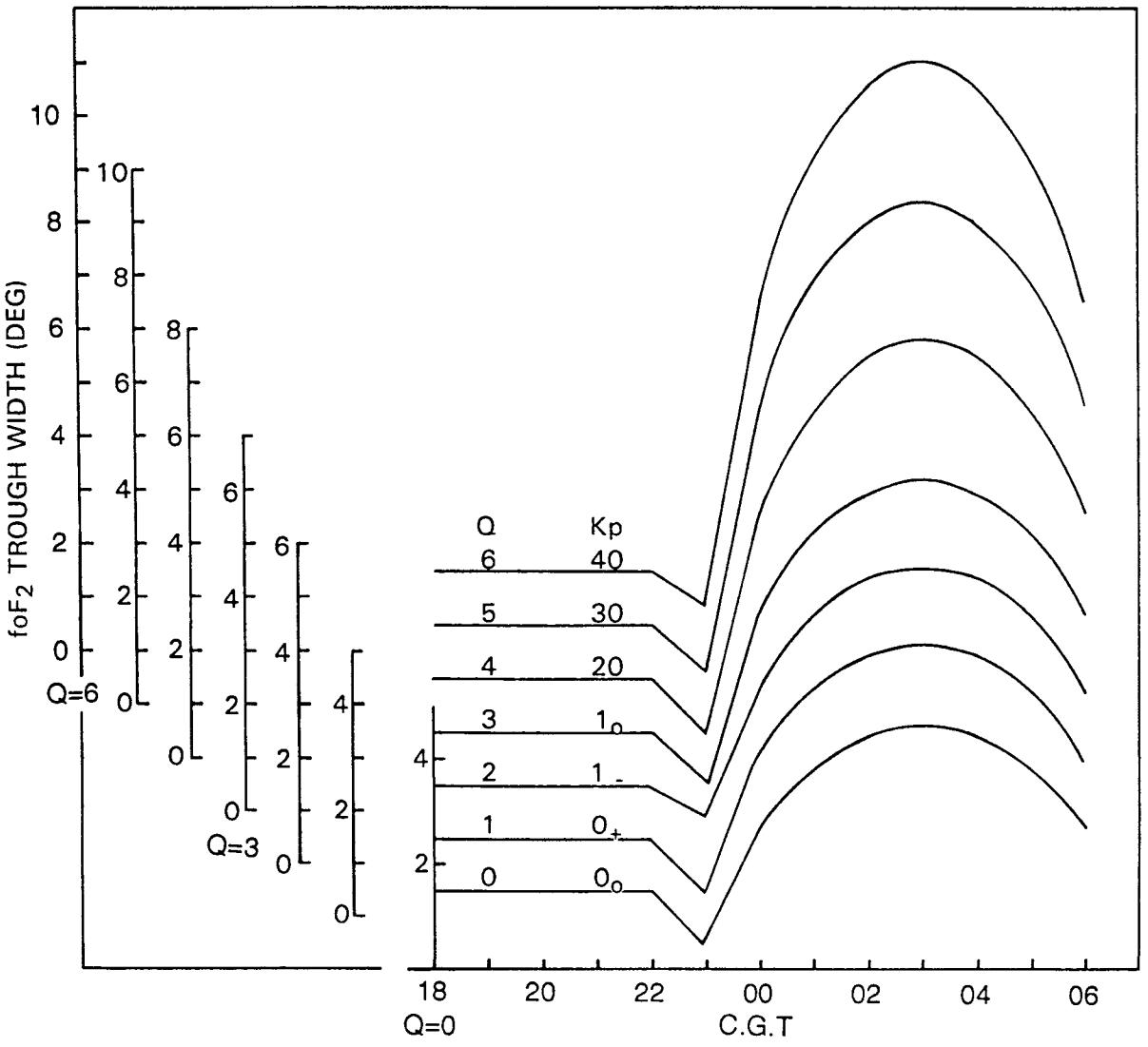

Figure 10 . Width of the Trough From the OTH Ionospheric Model.

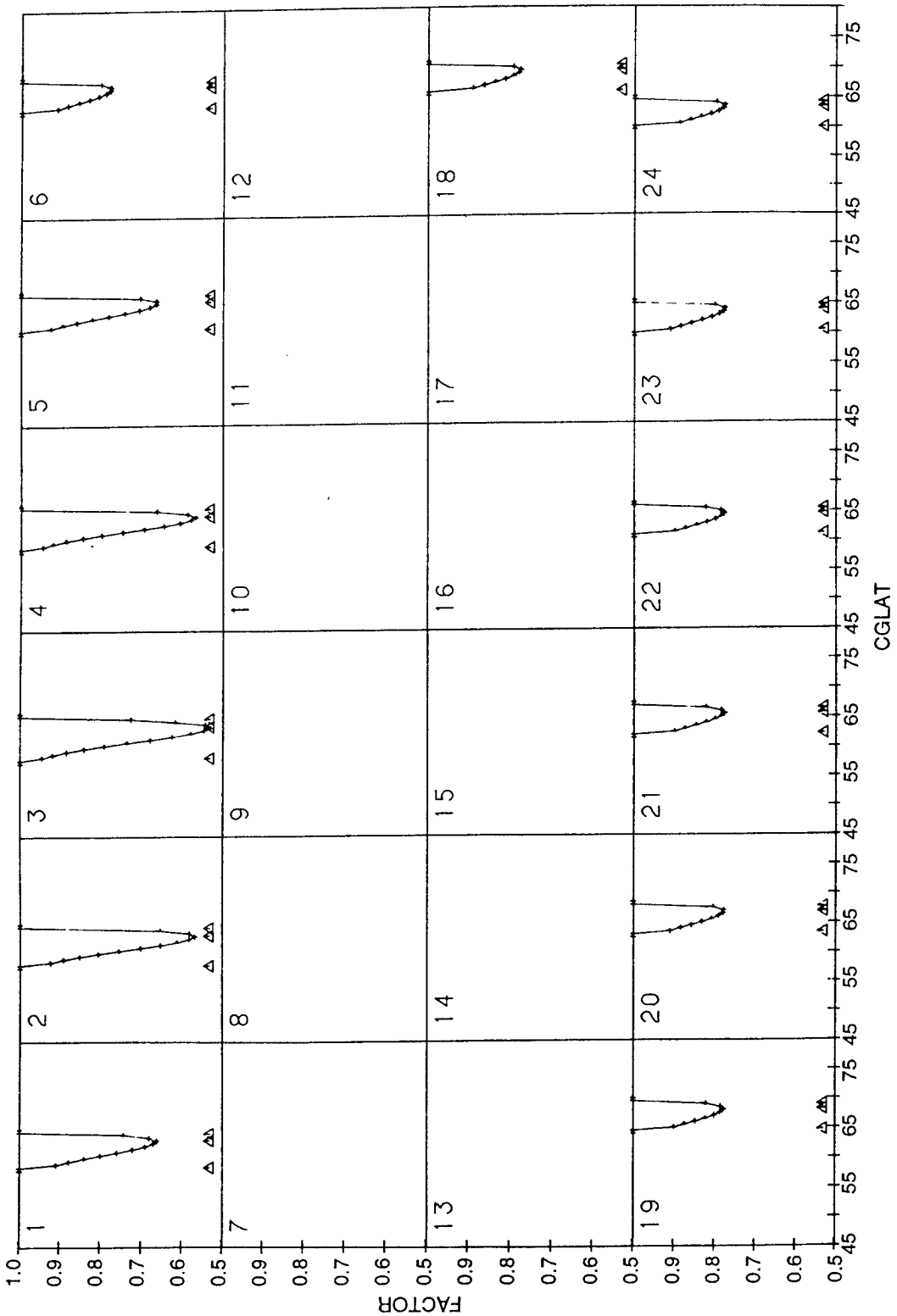

Figure 11. Modified Trough for Day 354 Using OTH Kp vs Q Relation for Q=3 (Kp=1).

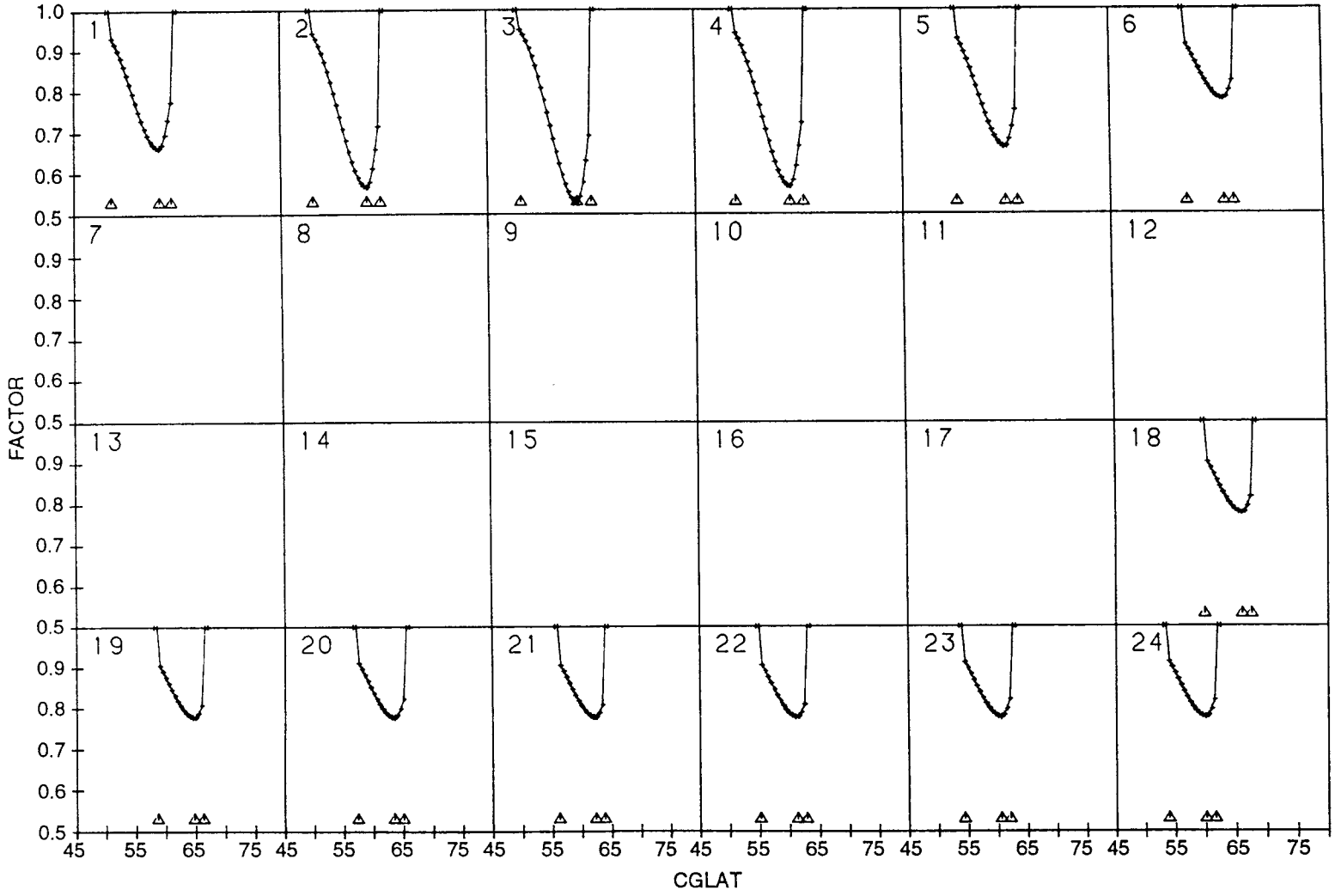

Figure 12. Modified Trough for Day 354 Using OTH Kp vs Q Relation for Q=6 (Kp=4).

3.3 Defining the foF_2 Trough From Observations

Observations have shown that the OTH ionospheric model foF_2 trough definition is inaccurate. The absence of the foF_2 trough from 1800-0000 CGMLT is not supported by the observations. On the other hand, the observations show that the foF_2 trough is well developed within 1 to 2 hours after sunset. An example of the foF_2 trough derived from the data recorded during an Airborne Ionospheric Observatory (AIO) flight on 2/3 March 1989, and from the simultaneous ground based observations, is shown in Figure 13. The data are presented in the CGM Local Time/Latitude coordinate system. The foF_2 contours show that the trough develops abruptly at 1930 CGMLT and is present at least up to 0230 CGMLT, the end of the AIO flight. The cross sections of the trough along CGM meridians are shown in hourly increments from the onset of trough development until 0000 CGMLT (Figure 14). The figure shows that the trough is well developed at 1930 CGMLT. As time progresses, the trough in general shows equatorward movement from 1930-0000 CGMLT. The trough wall on the poleward side (RHS) is steeper than that on the equatorward side (LHS). The movement of the equatorward wall is larger than that of the poleward wall. The trough is deeper when it is formed and becomes shallower with the general decay of the night time foF_2. Trough cross sections for two additional days are shown in Figures 15 and 16. These data and other available data sets clearly support the suggested modification of the OTH ionospheric model F layer trough.

3.4 K-AWS /Q_E Control of Trough and Auroral Oval

The F layer trough of the OTH ionospheric model is controlled by the 90 minute geomagnetic activity index K-AWS, provided in 90 minute increments by GWC. The auroral oval geometry and the auroral E and F layer enhancements are controlled by an effective oval diameter index Q_E, derived at GWC from satellite particle precipitation data.

Relationships between the magnetic Q index (for the discussion here equivalent to Q_E), Kp and K-AWS have been developed by AWS and Dandekar[13] (1982). These equations and the corresponding graphs are shown in Figure 17. The AWS set of equations is incorporated in the OTH ionospheric model, to permit the Q_E dependent oval diameter (equatorward oval boundary) to be determined from K-AWS in the absence of the GWC Q_E data that is, in the absence of the satellite data.

---

[13] Dandekar, B.S. *The statistical relations among Q, Kp and the Global Weather Central K-indices*, Environmental Research Papers, No. 763, AFGL-TR-82-0010, ADA118734.

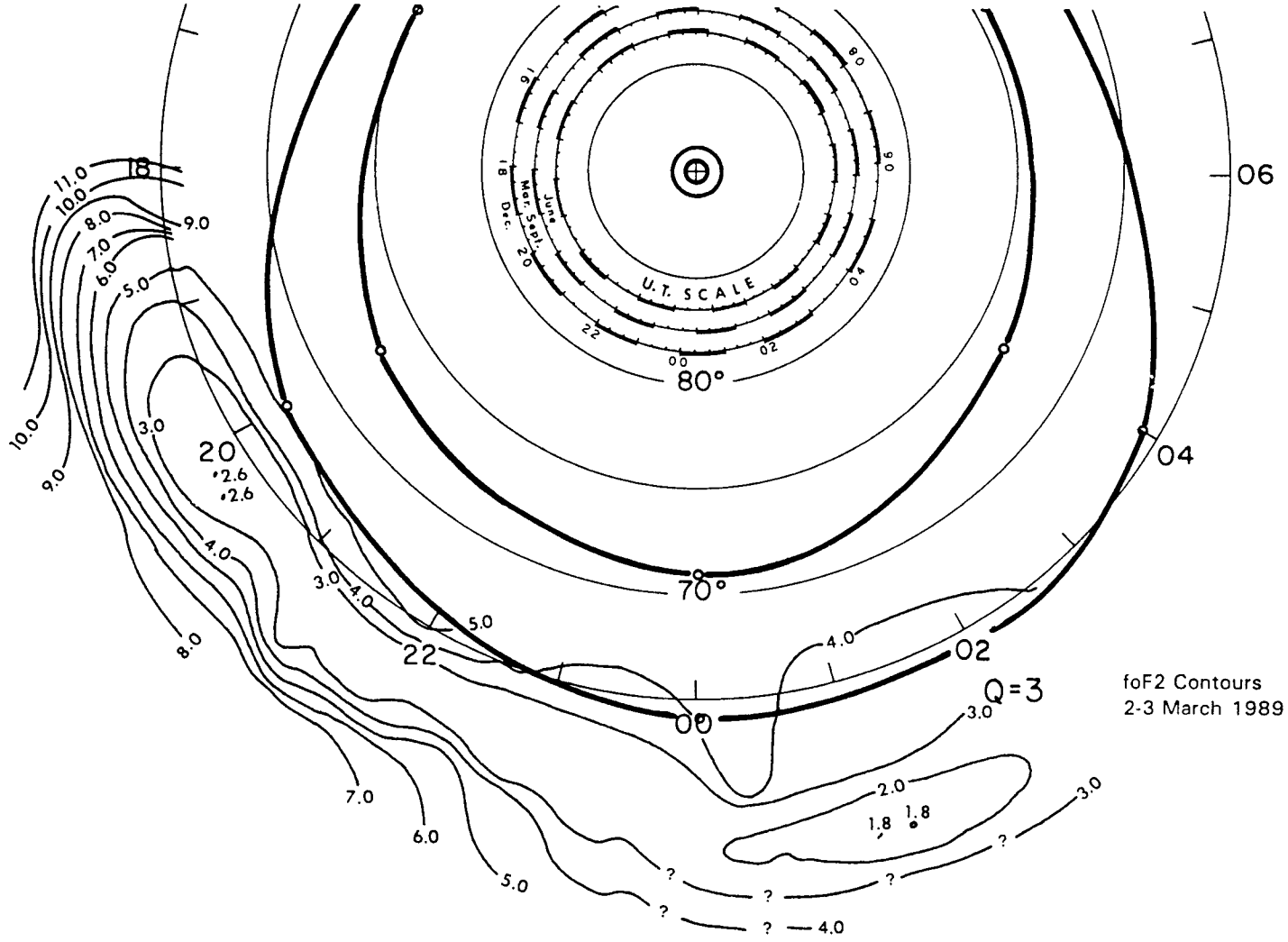

Figure 13. foF_2 Trough Observations on 2-3 March 1989 From AIO Flight and Ground Based Ionosonde Data.

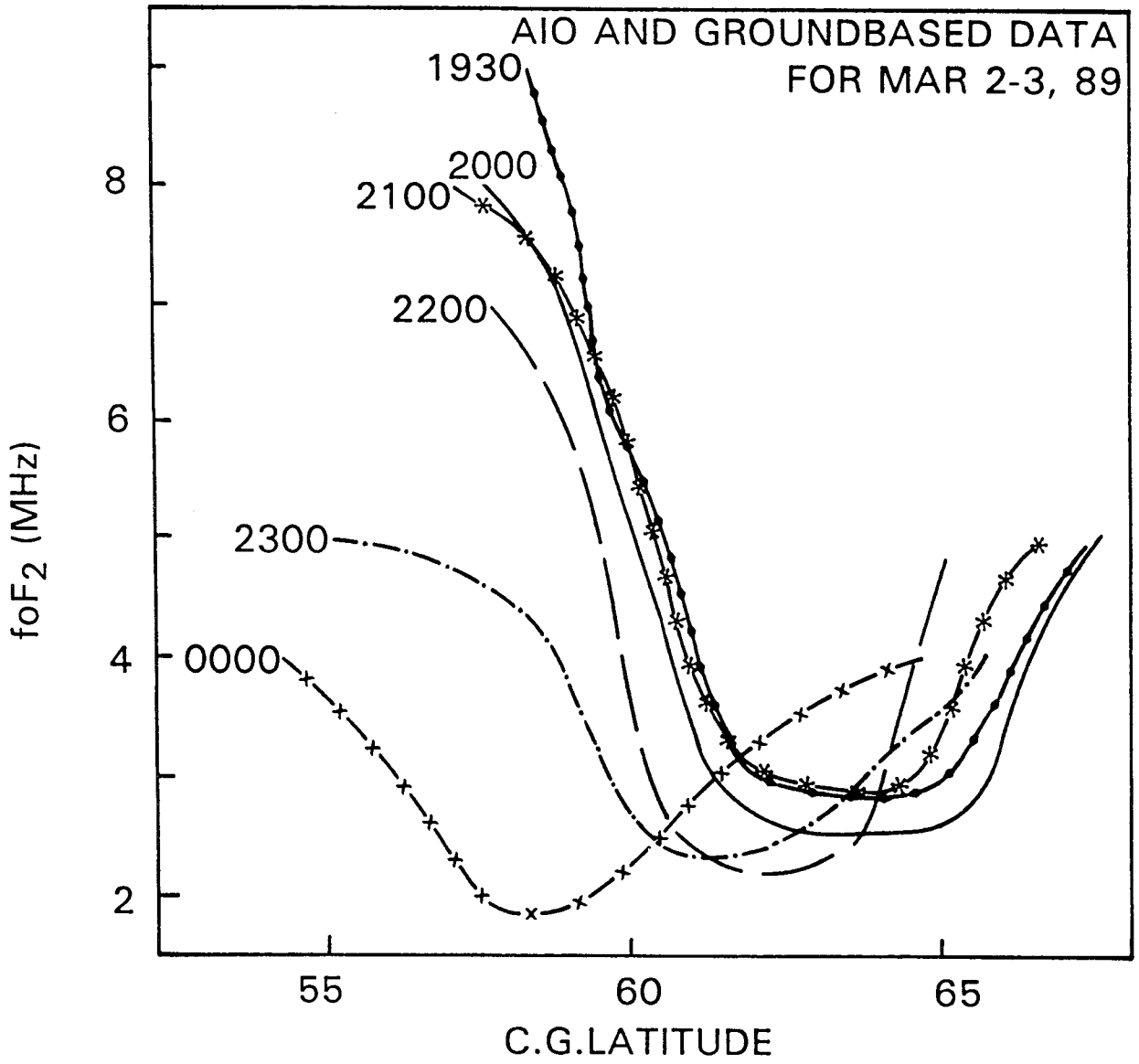

Figure 14. Longitudinal Cross-Sections of 2-3 March 1989 foF_2 Trough for Several Hours.

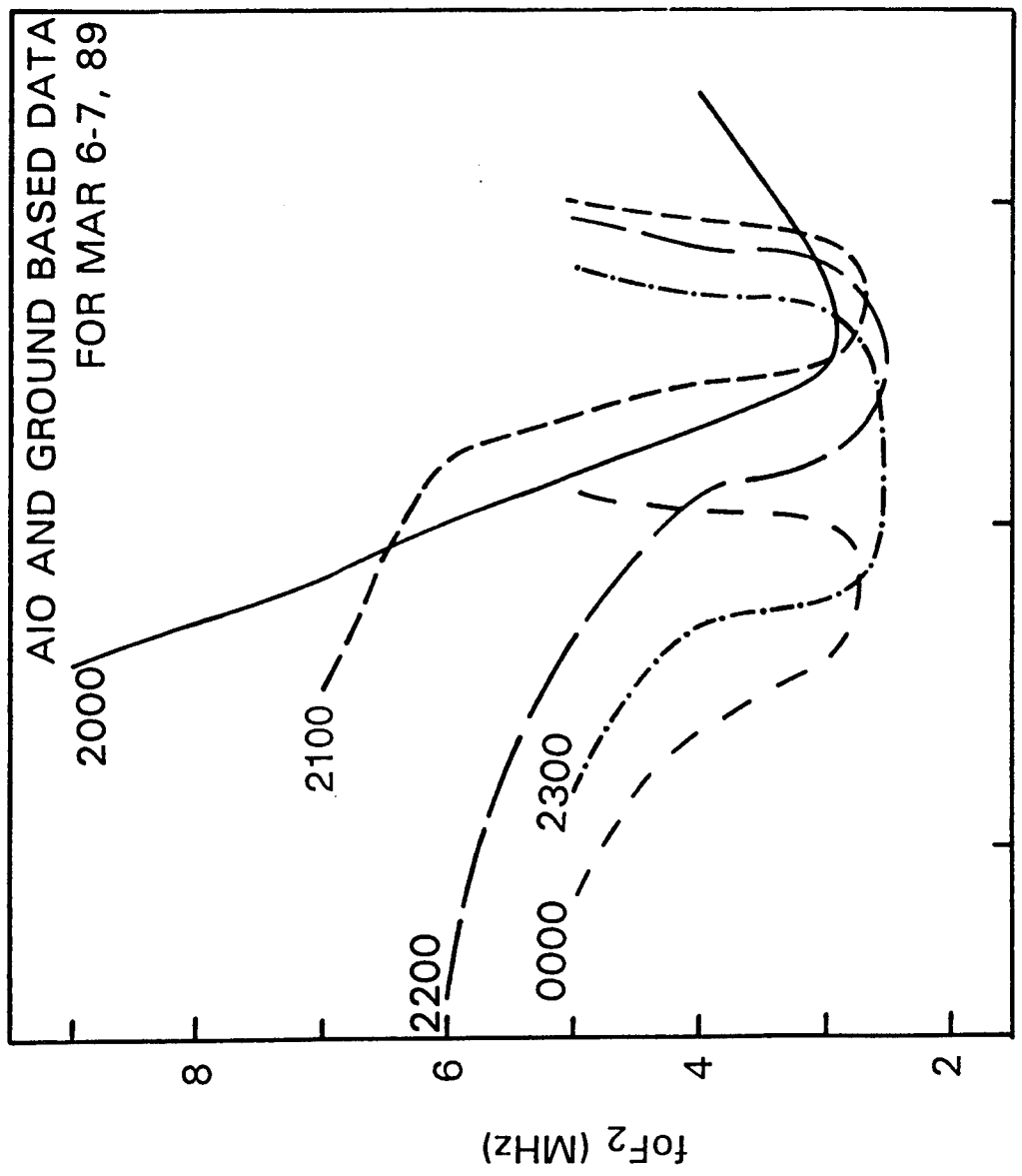

Figure 15. Longitudinal Cross-Sections of 6-7 March 1989 foF$_2$ Trough for Several Hours.

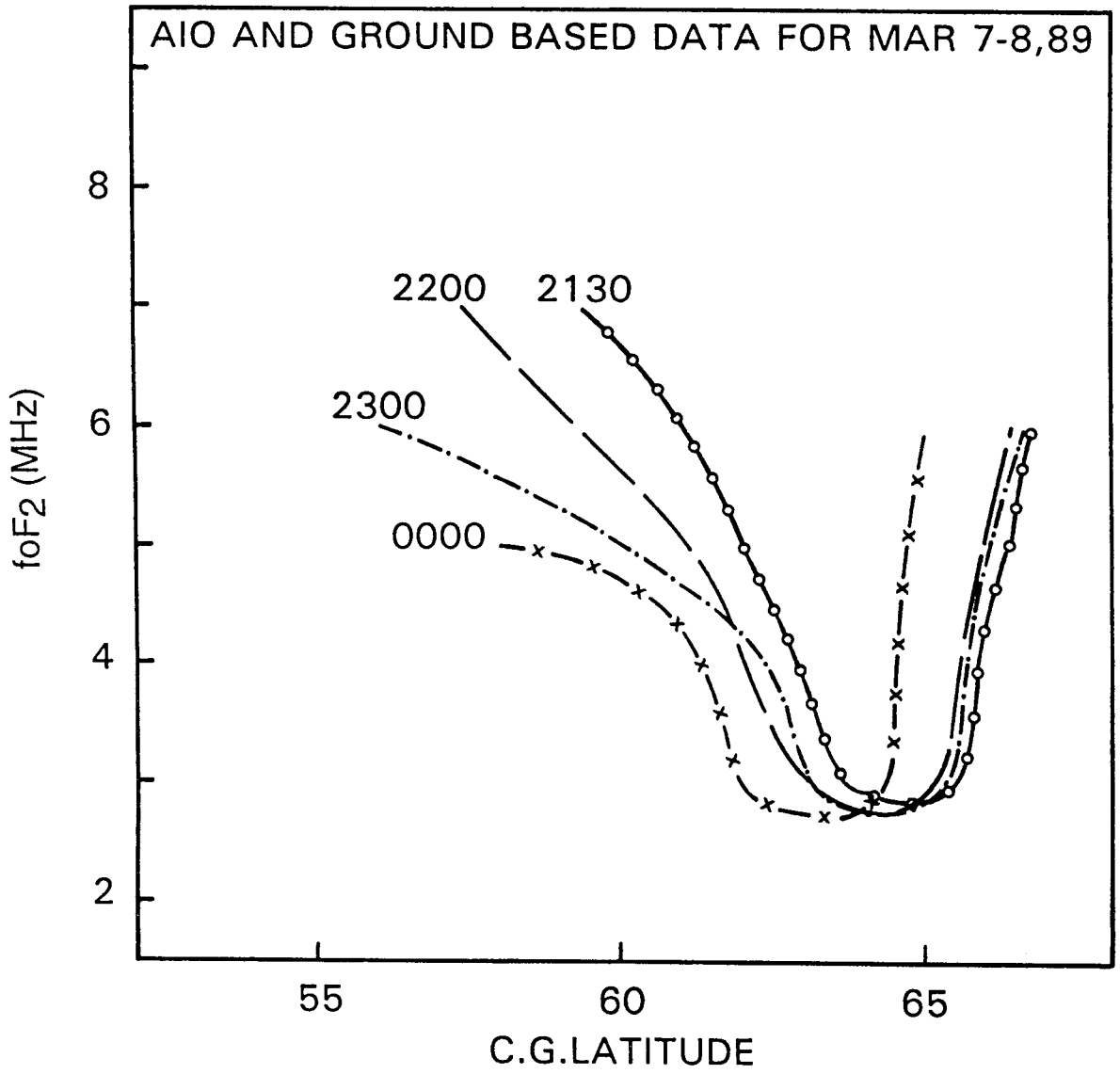

Figure 16. Longitudinal Cross-Sections of 7-8 March 1989 foF_2 Trough for Several Hours.

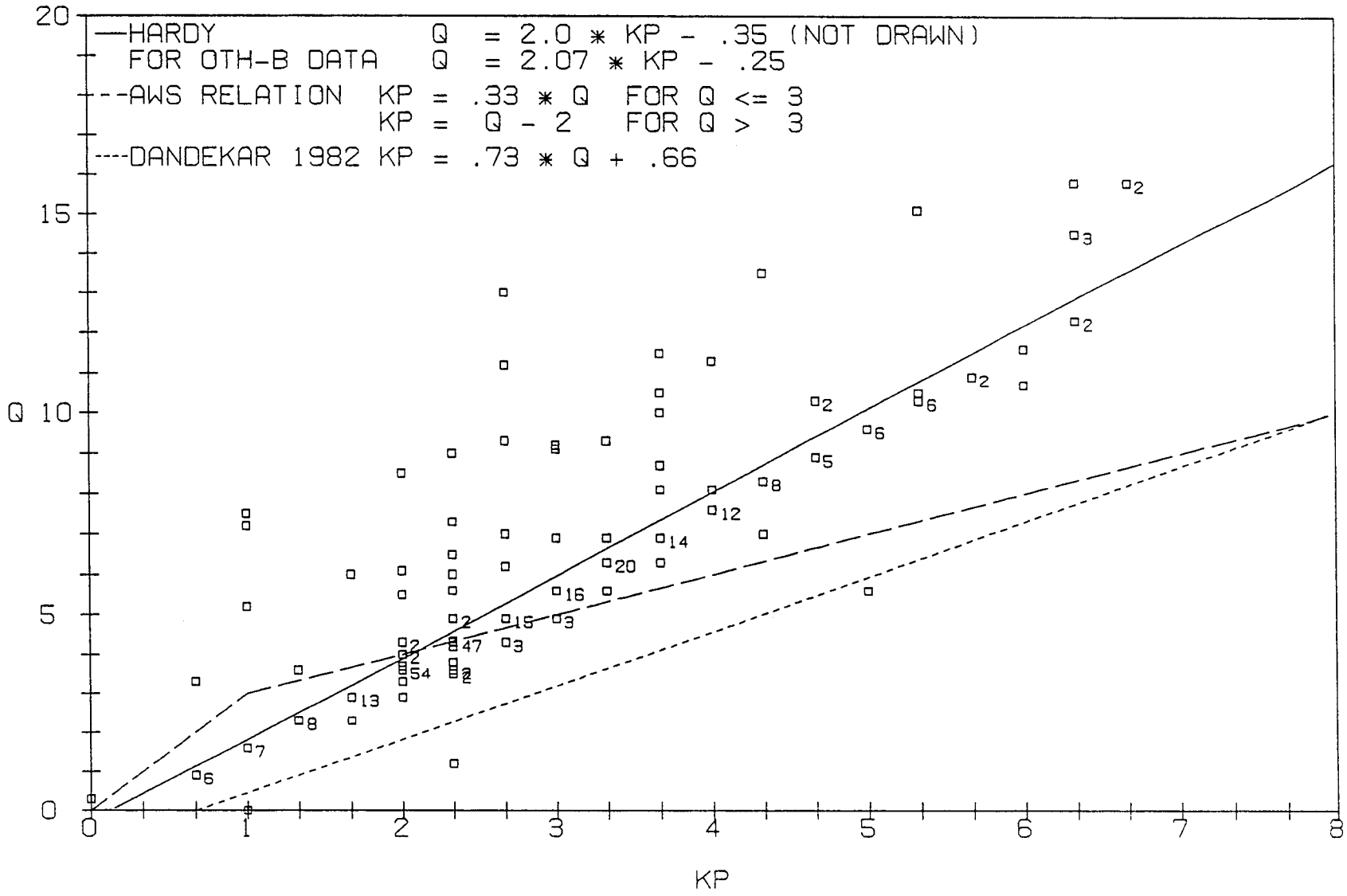

Figure 17. Kp vs Q Relation From AFGWC and Dandekar (1982). Solid line - least squares fit.

The current GWC procedure for the generation of Q_E from satellite particle precipitation data uses a set of CGM local time dependent equations of the precipitation boundary parameterized in Kp (Gussenhoven and Hardy 1983;[14] *AFGL Handbook of Geophysics and the Space Environment*, Chapter 12, 1985). When Q_E is not available from the particle precipitation data, it is derived from the ground based K-AWS index (available at 90 minute intervals using the Hardy (private communication) algorithm). The auroral boundary displayed at the ECRS/WCRS in the E/A model maps and displays the precipitation boundary, determined from the Gussenhoven-Hardy algorithms rather than the Starkov oval boundary used in the OTH ionospheric model. Its location is provided as a set of coordinate pairs in the AWS messages. The oval coincides with the precipitation boundary only in the midnight sector. In all other sectors the oval boundary is to the north of the precipitation boundary, farthest in the noon sector (~5°). (However, it should be noted that the OTH ionospheric model uses the oval boundary (Starkov equation) as the demarcation line between the trough and the auroral E and F layers. The AWS provided-Q_E is the parameter controlling the oval boundary.) A limited set of Q_E/K-AWS data available from several (DT&E) campaigns is shown in Figure 17 together with a least squared deviation fit straight line. When the data points superpose, the number on the right hand side lists the number of occurrences. The data clusters and the straight line fit very close to that of the Hardy algorithm indicate that most of these Q data are determined from the ground based K-AWS observations using the Hardy algorithm and not from the satellite borne particle precipitation data. It is clear that substantial differences exist between the three sets of equations relating the oval diameter index Q_E and K-AWS. Our observations also indicate a potential systematic overestimation of the oval diameter. We are currently investigating GWC procedures and the underlying assumptions and will provide an analysis of the problem in the near future.

In Table 2 in Millman et al.[1] the auroral latitudes listed under 2000 CGM time are too low by 2°. This error has occurred because the original Feldstein-Starkov[5] curves for this interval were plotted 2° too far south (drafting error). The interpolation scheme used in the model propagates the error proportionally over the 1630-2330 CGMLT sector. Therefore a 2° correction has to be added to the latitude values of 2000 CGMLT and the corresponding corrections should be applied for 1630 to 2330 CGMLT intervals in Table 2 of Millman et al.[1]

3.5 Updating the OTH Ionospheric Model With Real Time Vertical Incidence (VI) Site Data

The specification of the ionosphere by the OTH ionospheric model is improved by updating, using real time data from several Digisonde stations deployed in or close to the OTH coverage area. The procedure involves an interpolation scheme. As this information is

---

[14] Gussenhoven, M.S., Hardy, D.A. and Heinemann, N. (1983) Systematics of the equatorward diffuse auroral boundary, *J. Geophys. Res.*, **88**:5692.

not available in the published report (Millman et al.)[1] we used the OTH supporting document (unpublished private communication, Carl Bowser, GE) for this discussion.

The interpolation scheme is based on a correlation study by Rush and Gibbs[15] (1973) using data from N-S and E-W (geomagnetic) chains of ionospheric stations. The weight factors used in the interpolation scheme are the correlation coefficients, which are q=1 at the Vertical Incidence (VI) sounder sites (separation 0 nmi) and which decrease to q=0 as the separation between the VI sites increases to a certain range, at which the ionospheric variations at the two sites become uncorrelated (independent). For foF_2 and M(3000) Rush and Gibbs (1973) observed that for a given station these correlation distances are different in the E-W and N-S direction and they show a very strong seasonal dependence.

In the OTH ionospheric model, the base model is the ITS-78 (Barghausen et al.[16] 1969) which needs the sunspot number, Julian day and Universal Time. To adjust the ITS-78 for specification purposes AFGWC determines an effective sunspot number SSN_{eff} from the past five days' foF_2 observations from a network of 50 VI ionospheric stations. This SSN_{eff} is used to drive the ionospheric model providing a best fit to the global data. On the base model auroral E and F layer enhancements (function of Q index) and F layer trough (function of Kp) are superposed. The resulting model is the AFGWC polar ionospheric model. A second correction is then applied that uses real time data from local sounder stations in the vicinity of the coverage area.

The interpolation scheme uses the model parameters predicted for a given hour. It computes the percent change between the observation and the prediction of a given parameter at the ionospheric station providing the data. To the grid points in the vicinity of that site a fraction of the observed change is applied. The fraction is computed as the correlation coefficient (Rush and Gibbs),[15] which is a function of the separation distance between the VI site and the grid point. In this way all the grid points in the coverage area are updated. Such updated predictions based on real time observations would indeed be more realistic than the simple 'effective sunspot SSN_{eff} ' driven model result.

In using this approach the OTH ionospheric model suffers from several errors.

(1) *Presentation of correlation coefficients.* As the weight factors are different along the E-W and N-S directions (Rush and Gibbs 1973), the shape of the weight factors as a function of distance between the grid point and the VI site will be an ellipse. The curve determined from Eq. (90-41) (p. 1878 unpublished report by Carl Bowser) is shown in Figure 18. Two items to be noted in Figure 18 are: a) the weight factor peaks at a certain distance away from the VI site (located at (0.0)) and b) the curve is not

---

[15] Rush, C.M. and Gibbs (1973) Predicting the day-to-day variability of the mid-latitude ionosphere for applications to HF propagation predictions, *Air Force Surveys in Geophysics No. 268*, May, AFCRL-TR-73-0335, AD764711.

[16] Barghausen, A.F., Finney, J.W., Proctor, L.W. and Schultz, L.D. (1969) Predicting long-term operational parameters of high frequency sky wave telecommunication systems, *ESSA Technical Report ERL 110-ITS-78*, Washington, DC.

elliptical. In the computer program the values greater than 1 are set equal to 1, but this does not alter the shape of the curves in Figure 18.

(2) *Assignment of areas of updating to Vertical Incidence (VI) sites.* The scheme uses at most two stations for updating a given grid point and assigns somewhat arbitrary areas to the individual VI sites. The VI sites used/planned for the OTH update are listed in Table 1. Figure 19a shows the OTH coverage area and the locations of the VI sites currently included in the updating scheme. Additional Digital Ionospheric Sounding System (DISS) stations of importance to the East Coast Radar System (ECRS) model update are now available since the deployment of DISS at Sondrestrom and Narsarssauq, Greenland and at Ramey AFB, Puerto Rico. The OTH coverage area is broken into segments (1-3) and sectors (1-8 in each segment) for which the identified stations provide primary update (Figure 19a). Of these the Azores site will not be established, while Patrick AFB and Croughton, UK have not yet become operational. Goose Bay, Argentia, and Bermuda are inside the OTH coverage area while Bangor, Wallops Island, and Patrick AFB are on the border of the coverage area. The closest grid point of the radar coverage area is 450 nm away from the VI site Croughton, UK. For Croughton the program uses 1-1/2 hour old data to update foF_2 in the coverage, but fails to transfer the VI site to the appropriate (22.5° West of Croughton) location, into the coverage area of the radar. As it is, it introduces an unwanted error due to the diurnal variation at Croughton over the 1-1/2 hour time interval. Figure 19b shows the area allocation of secondary VI sites. The allocation of the grid points to the VI sites used by the OTH model from Table XLII p.1882 (Carl Bowser unpublished report), for updating are listed in Table 2. The primary sites are not underlined. The secondary sites are underlined. The grid point closest to the VI site is marked by '*'. Note that the sites 2, 4, and 6 are used as secondary in their own immediate vicinity.

Table 1. Vertical Incidence (VI) Update Sites for East Coast Radar System Coverage

NO	STATION NAME	GEOGRAPHIC		θ°
		LAT.	LONG.	
0	BANGOR, USA	44.98	291.18	3.9
1	THULE, GREENLAND	76.50	291.33	31.4
2	GOOSE BAY, CANADA	53.31	299.40	7.9
3	CROUGHTON, UK	52.00	358.83	16.4
4	ARGENTIA, CANADA	47.29	306.03	8.4
5	SAN MIGUAL ISLAND, AZORES	38.00	335.00	11.5
6	HAMILTON, BERMUDA	32.33	295.33	3.4
7	WALLOPS ISLAND, USA	38.00	284.50	1.7
8	PATRICK AFB, USA	28.17	279.33	0.3

Table 2. (from Table XLII p. 1882 Carl Bowser unpublished report) Grid Point Assignment to Primary and Secondary VI Sites (Only Secondary are Underlined)

SEC/ SEG	1	2	3	4	5	6	7	8	9	10	11	12	13	14	15	16	17	18	19	20	21	ONE	TWO
1-1	0,	0,	0,2	0,2	2,	2,	2,	2,	2,	2,	2,	2,	2,	2,	2,	2,	2,	2,	2,	2,	2,	19	2
1-2	0,	0,	0,2	0,2	2*,	2,	2,	2,	2,	2,	2,	2,	2,	2,	2,	2,	2,	2,	2,	2,	2,	19	2
1-3	0,	0,	0,2	0,2	2,	2,	2,	2,	2,	2,	2,	2,	2,	2,	2,	2,	2,	2,	2,	2,	2,	19	2
1-4	0,	0,	0,2	0,2	2,	2,	2,	2,	2,	2,	2,	2,	2,	2,	2,	2,	2,	2,	2,	2,	2,	19	2
1-5	0,	0,	2,4	2,4	2,4	2,4	2,4	2,4	2,4	2,4	2,4	2,4	2,4	2,4	2,4	2,4	2,4	2,4	2,4	2,4	2,4	2	19
1-6	0,	0,	2,4	2,4	2,4	2,4	2,4	2,4	2,4	2,4	2,4	2,4	3,	3,	3,	3,	3,	3,	3,	3,	3*,	11	10
1-7	0,	0,	0,4	0,4	4,	4,	4,	4,	3,4	3,4	3,4	3,4	3,	3,	3,	3,	3,	3,	3,	3,	3,	15	6
1-8	0,	0,	0,4	0,4	4*,	4,	4,	4,	3,4	3,4	3,4	3,4	3,	3,	3,	3,	3,	3,	3,	3,	3,	15	6
2-1	0,	0,	0,4	0,4	4,	4,	4,	4,	3,4	3,4	3,4	3,4	5,	5,	5,	5,	5,	5,	5,	5,	5,	15	6
2-2	0,	0,	0,4	0,4	4,	4,	4,	4,	3,4	3,4	3,4	3,4	5,	5,	5,	5,	5,	5,	5*,	5,	5,	15	6
2-3	0,	0,	0,4	0,4	4,	4,	4,	4,	4,	4,	4,	4,	4,	5,	5,	5,	5,	5,	5,	5,	5,	19	2
2-4	0,	0,	0,4	0,4	4,	4,	4,	4,	4,	4,	4,	4,	4,	5,	5,	5,	5,	5,	5,	5,	5,	19	2
2-5	0,	0,	0,4	0,4	4,	4,	4,	4,	4,	4,	4,	4,	4,	5,	5,	5,	5,	5,	5,	5,	5,	19	2
2-6	0,	0,	0,	0,	7,	7,	7,	7,	6,	6,	6,	6,	6,	6,	6,	6,	6,	6,	6,	6,	6,	21	0
2-7	0,	0,	0,	0,	7,	7,	7,	7,	6,	6,	6,	6,	6,	6,	6,	6,	6,	6,	6,	6,	6,	21	0
2-8	0,	0,	0,	0,	7,	7,	7,	7,	6,	6,	6,	6,	6,	6,	6,	6,	6,	6,	6,	6,	6,	21	0
3-1	0,	0,	6,7	6,7	6,7	6,7	6,7	6,7	6,	6,	6,	6,	6,	6,	6,	6,	6,	6,	6,	6,	6,	15	6
3-2	0,	0,	6,7	6,7	6,7	6,7	6,7	6,7	6,	6,	6,	6,	6,	6,	6,	6,	6,	6,	6,	6,	6,	15	6
3-3	0,	0,	6,7	6,7	6,7	6,7	6,7	6,7	6,	6,	6,	6,	6,	6,	6,	6,	6,	6,	6,	6,	6,	15	6
3-4	0,	0,	6,7	6,7	6,7	6,7	6*,7	6,7	6,	6,	6,	6,	6,	6,	6,	6,	6,	6,	6,	6,	6,	15	6
3-5	0,	0,	6,7	6,7	6,7	6,7	6,7	6,7	6,	6,	6,	6,	6,	6,	6,	6,	6,	6,	6,	6,	6,	15	6
3-6	0,	0,	6,7	6,7	6,7	6,7	6,7	6,8	6,8	6,8	6,8	6,8	6,8	6,8	6,8	6,8	6,8	6,8	6,8	6,8	6,8	2	19
3-7	0,	0,	6,7	6,7	6,7	6,7	6,7	6,8	6,8	6,8	6,8	6,8	6,8	6,8	6,8	6,8	6,8	6,8	6,8	6,8	6,8	2	19
3-8	0,	0,	6,7	6,7	6,7	6,7	6,7	6,8	6,8	6,8	6,8	6,8	6,8	6,8	6,8	6,8	6,8	6,8	6,8	6,8	6,8	2	19
R-1	0,	0,	6,7	6,7*	6,7	6,7	6,7	6,8	6,8	6,8	6,8	6,8	6,8	6,8	6,8	6,8	6,8	6,8	6,8	6,8	6,8*	2	19
R-2	0,	0,	0,	0,	0,	0,	0,	0,	0,	0,	0,	0,	0,	0,	0,	0,	0,	0,	0,	0,	0,	NA	
R-3	0*,	0,	0,2	0,2	2,	2,	2,	2,	2,	2,	2,	1,	1,	1,	1,	1,	1,	1*,	1,1	1,	1,	NA	
R-4	0,	0,	0,2	0,2	2,	2,	2,	2,	2,	2,	2,	2,	2,	2,	2,	2,	2,	2,	2,	2,	2,	19	2
																				TOTAL		371	175
																				PERCENT		68	32

0-BANGOR, 1-THULE, 2-GOOSE BAY, 3-CROUGHTON, 4=ARGENTIA
5-AZORES, 6-BERMUDA, 7-WALLOPS ISLAND, 8-PATRICK AFB
BEAMS R-2 (270°W), R-3 (0°N) ARE OUTSIDE THE COVERAGE AREA.
Grid-point 1 is 200 nm away from the transmitter

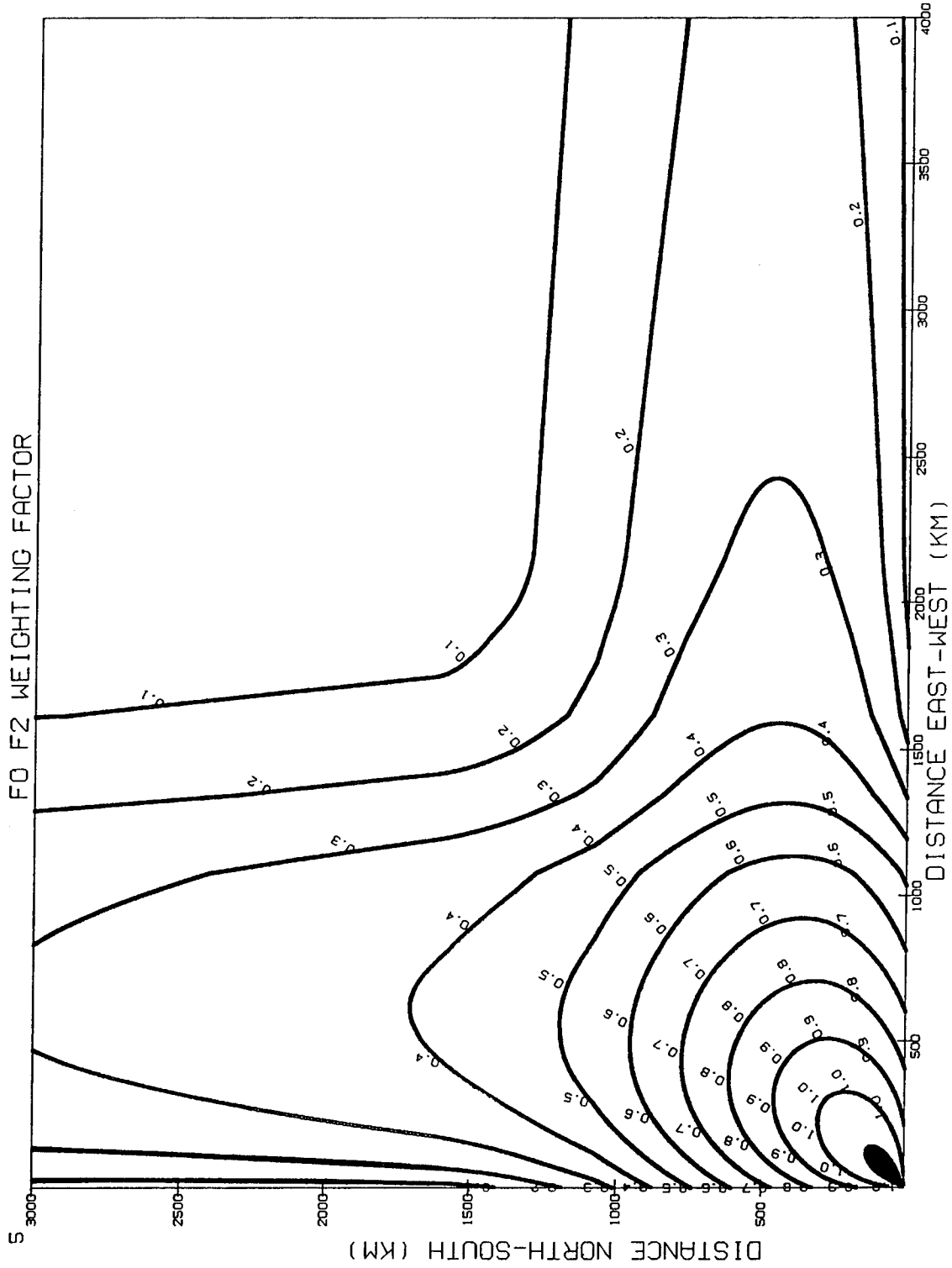

Figure 18. Weight Factor Determined From OTH GE Model for foF_2 for December-February Period.

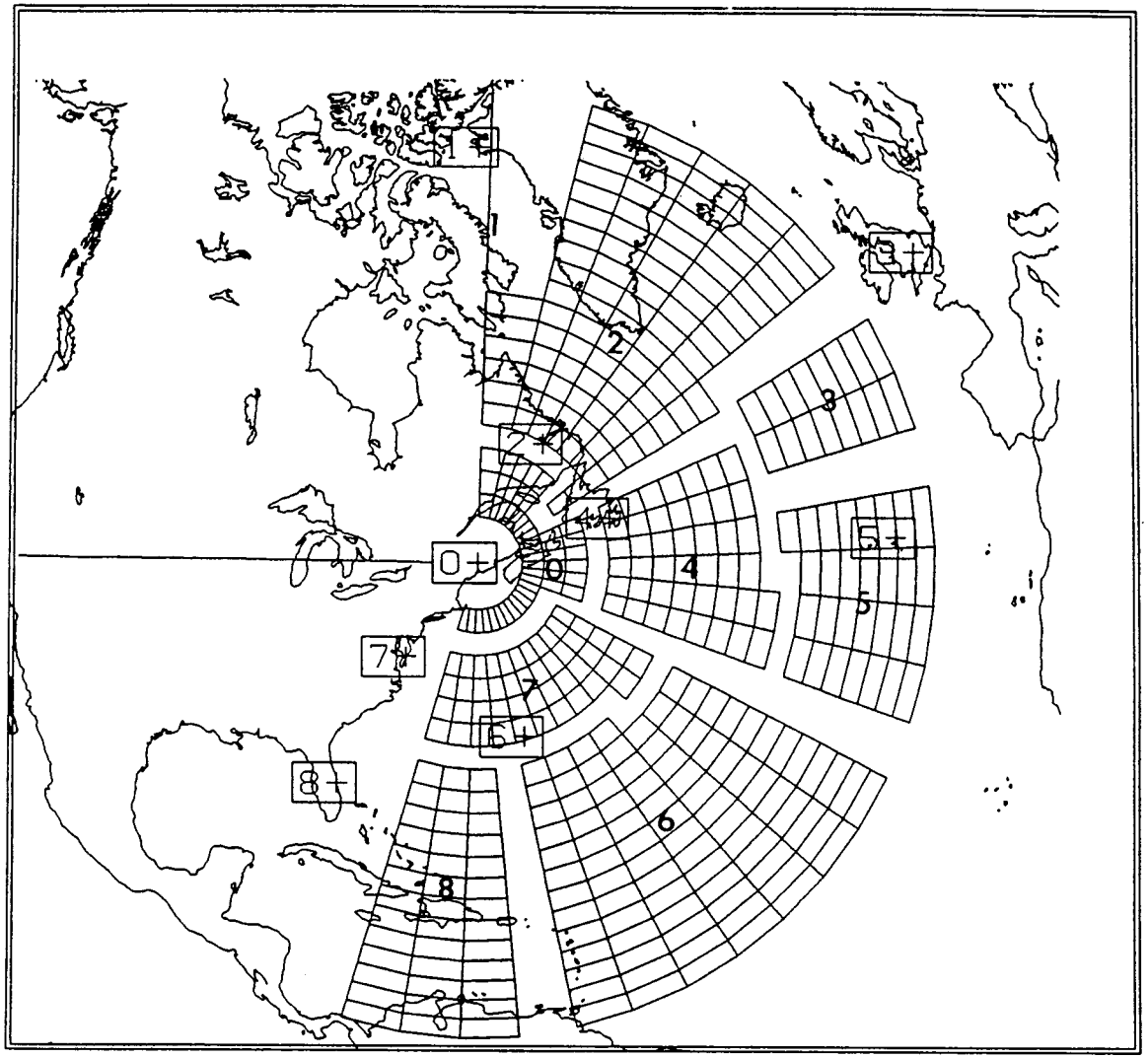

Figure 19a. OTH Coverage Area, Showing the Locations of Vertical Incidence Sites and Regions Allotted to the Respective VI sites Where That Site Will be the Primary Source for Updating Ionospheric Parameters.

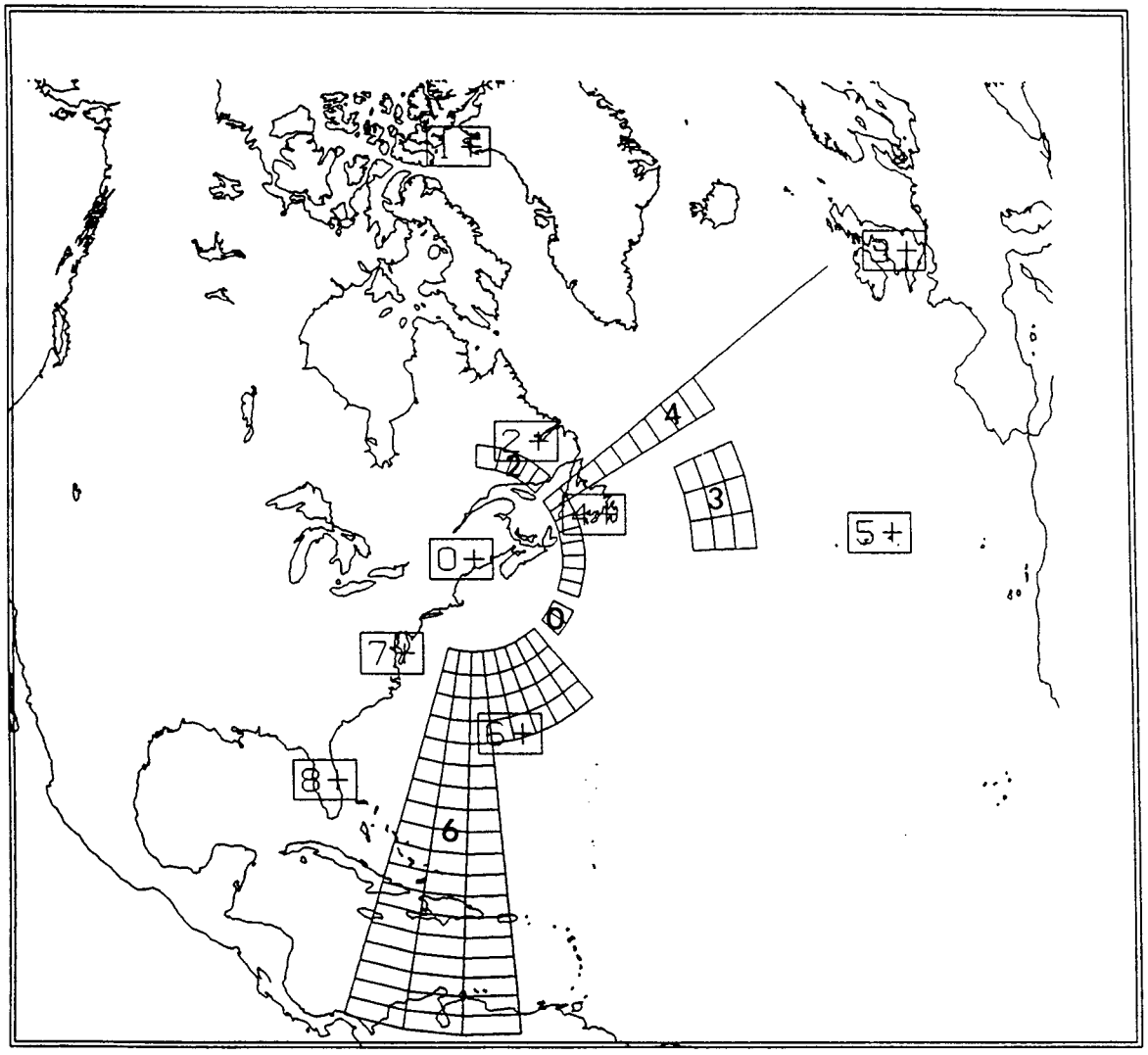

Figure 19b. OTH Coverage Area, Showing the Locations of Secondary VI Sites Used for Updating the Model Data at the Grid Points.

Figures 19a and 19b and Table 2 show that the assignment of the areas to the respective DISS stations is somewhat arbitrary. While the present area assignments prevent the stations in the north from influencing areas in the south (that is, trough stations cannot influence the midlatitude ionosphere), it also prevents the smoothing of the resulting model by the joint use of the available updating data base during times when all stations are in a very similar ionosphere, namely during daytime, when all stations are under the influence of the midlatitude ionosphere.

Special problems arise with the current scheme, if the updating data base is incomplete. Non-availability of data from certain stations (for example, Argentia, station 4) will lead to unreliable updates (fallback to five days' average) over large irregular areas with possible sharp transitions at the borders.

A look at Table 2 shows that only 32 percent of the grid points are updated by two VI sites, while a large fraction (68 percent) have to rely on a single update.

(3) *Update using two Vertical Incidence (VI) sites.* The two-site weight factors K'_1 and K'_2 listed in Eqs. (90-45, 46) are defined on pp1879-80 (Carl Bowser unpublished report). These are:

$$K'_1 = \frac{q'_{01} - q'_{02} * q'_{12}}{1 - q'^2_{12}} \qquad (90\text{-}45)$$

$$K'_2 = \frac{q'_{02} - q'_{01} * q'_{12}}{1 - q'^2_{12}} \qquad (90\text{-}46).$$

The use of an incorrect equation for the weight factor (refer to Figure 18) yields incorrect values for q'_{01}, q'_{02}, and q'_{12}. Also, when the denominator $1-q'^2_{12}$ approaches zero, these equations can yield large positive and negative values for K'_1.

The K'_1 values computed from this GE model can be positive and negative as shown in Table 3. In Table 3 the left hand column lists the segment and the sector (beam) number of a grid point. The remaining columns at the top refer to the grid point number along a ray. The first grid point is 200 nmi from the transmitter site. The consecutive beams are separated by 7.5° in azimuth. Notice in columns 10 and 11 that the first two weight factor pairs have comparable magnitudes but opposite signs. Also along segment 1 sector 5, the grid points 5 and 7 have K' values of 0.502, but the grid point number 6 between the two has the K' value 2.120. Such discontinuous values result in errors in the update.

To avoid an infinite value of K' it is arbitrarily set to 0.5 when the denominator in Eqs. (90-44), and (90-45) is zero, in the respective computer program.

Table 3. Weight Factor K for Two Station Update

foF_2 90-45 WEIGHTING FACTOR FOR 2 VI SITE UPDATE SEASON 3 MAY, JUN, JUL, AUG

GRID POINT	1	2	3	4	5	6	7	8	9	10	11
SC 1 BM 1	....	....	0.000	0.000	....	....	....	....	....	....	....
SC 1 BM 2	....	....	0.000	0.000	....	....	....	....	....	....	....
SC 1 BM 3	....	....	0.000	0.000	....	....	....	....	....	....	....
SC 1 BM 4	....	....	0.000	0.011	....	....	....	....	....	....	....
SC 1 BM 5	....	....	0.502	0.502	0.502	2.120	0.502	0.502	0.181	-1.676	-2.282
SC 1 BM 6	....	....	-2.661	0.502	0.502	0.502	0.502	0.502	0.502	2.481	3.920
SC 1 BM 7	....	....	0.379	0.264	....	....	....	....	0.682	0.675	0.658
SC 1 BM 8	....	....	0.299	0.108	....	....	....	....	0.930	0.918	0.892
SC 2 BM 1	....	....	0.345	0.247	....	....	....	....	0.993	0.994	1.002
SC 2 BM 2	....	....	0.426	0.391	....	....	....	....	1.075	1.088	1.028
SC 2 BM 3	....	....	0.545	0.500	....	....	....	....	....	....	....
SC 2 BM 4	....	....	0.551	0.551	....	....	....	....	....	....	....
SC 2 BM 5	....	....	0.551	0.551	....	....	....	....	....	....	....
SC 2 BM 6	....	....	-0.065	-0.097	....	....	....	....	....	....	....
SC 2 BM 7	....	....	-0.068	-0.102	....	....	....	....	....	....	....
SC 2 BM 8	....	....	-0.071	-0.107	....	....	....	....	....	....	....
SC 3 BM 1	....	....	-2.439	-3.814	-2.859	-2.394	-1.151	....	....	....	....
SC 3 BM 2	....	....	-1.952	-2.986	-1.977	-1.499	-0.429	....	....	....	....
SC 3 BM 3	....	....	-0.834	-2.207	-1.139	-0.653	0.460	....	....	....	....
SC 3 BM 4	....	....	-0.377	0.823	-0.292	0.146	0.152	....	....	....	....
SC 3 BM 5	....	....	-1.864	-0.685	0.494	0.505	0.505	....	....	....	....
SC 3 BM 6	....	....	-2.460	0.069	0.505	0.505	0.505	-0.010	-0.235	-0.141	0.051
SC 3 BM 7	....	....	-1.879	0.505	0.505	0.505	1.813	0.155	-0.075	0.018	0.252
SC 3 BM 8	....	....	-1.038	0.505	0.505	0.776	3.157	0.413	0.120	0.166	0.469
REFERN 01	....	....	0.118	0.505	0.505	1.489	3.593	0.820	0.551	0.350	0.626
REFERN 02	....	....	....	....	....	....	....	....	....	....	....
REFERN 03	....	....	-0.015	-0.053	....	....	....	....	....	....	....
REFERN 04	....	....	0.000	-0.010	....	....	....	....	....	....	....

These weight factors were proposed by Gautier and Zacharisen[17] (1985) for predicting variations at a given station from the observations at the other station (or at a later time for the same station) provided the seasonal and diurnal standard variations at each hour at both stations are known. Since these standard variations are not known for the pairs of the OTH grid point and the VI site, these equations should not be used.

Corrected values for K'_i were computed from the above equations with the proper system of coordinates (geographic in place of geomagnetic) used for computation of distance of a grid point from a VI site and the use of an ellipse (see next section) instead of Eq. (90-41) (p.1878 Carl Bowser unpublished report) for weight factors. With this approach the joint weight factors K'_i and K'_{ii} for the stations 'i' and 'ii' show a slow reduction with increasing distance of the grid points from the paired VI sites and one of the values (either K'_i or K'_{ii} but not both) may be negative, but for the given pair the difference between the two is positive. An explanation for this is: depending on the separation between the pair of updating VI sites the redundancy of correction by each site is reduced (negative K') by an appropriate fraction. We are proposing use of all available sites for updating instead of the two station limit of the present approach. The K' factors need to be computed for multiple station updates. Gautier and Zacharisen[17] have presented an elaborate method for computing K' factors for a multiple station update. A rather simple method for replacing K'_i is proposed in the following section.

(4) *Separation between Vertical Incidence (VI) site and the grid point.* To determine the separation between the VI site and grid point the OTH model uses the geomagnetic coordinate system, which results in incorrect separation distances, leading to incorrect weight factors (from Eq. (90-41) p1878, Carl Bowser unpublished report). This is due to the fact that the geomagnetic coordinate system is distorted with respect to the geographic coordinate system.

4. PROPOSED CORRECTIONS/MODIFICATIONS OF OTH MODEL

To correct errors in procedure and shortcomings in the updating process, the following steps are suggested:

1. Correct the presentation of the correlation function (ellipse).

---

[17] Gautier, T.N. and Zacharisen, D.H. (1965) *Use of Space and Time Correlation in Short-term Ionospheric Predictions*, First Annual IEEE Communications Convention, Boulder, Colorado, June 7-9, pp. 671-676.

2. Allow all available DISS stations and the radar's own VI sounder to participate in the updating process at all the grid points in the OTH coverage area ionosphere according to their distances to the respective updating location and the phenomenon.

3. Modify the two/multiple station updating procedure with a simple algorithm.

4. To prevent sub-oval stations from updating the auroral and trough F-layers and vice versa, we propose to use the Q_E Starkov equatorward oval boundary and the K-AWS trough boundary to determine the northward extent of influence of sub-trough stations, and the southward influence of the oval stations.

5. The trough will be updated only by stations like Goose Bay and/or Argentia, which have actually moved into the trough region as defined by the location of the equatorward boundary of the oval and of the equatorward boundary of the trough. The trough is bounded by the 1800 (through 0000) and 0600 CGMLT meridians.

Specifically, Goose Bay and/or Argentia move from the midlatitude ionosphere in the daytime, into the trough ionosphere after sunset, and into the oval at a time depending on Q_E. We propose here to let Goose Bay and Argentia update the midlatitude ionosphere in the daytime according to the weight of the correlation function. As the Q_E/K-AWS defined oval/and trough move into the coverage area, the trough/oval area will not be updated by the DISS stations, since at this early time no DISS will be in or even close to these regions. Goose Bay and Argentia will only affect the trough or oval ionosphere if the specified trough or oval boundary is south of the respective station. The influence of the stations on the updating process will then be limited to the respective (trough or oval) regime.

Presentation of correlation coefficients: The Eq. (90-41) p.1878 (Carl Bowser unpublished report) is replaced by the equation of an ellipse using the following procedure. The equation of an ellipse is given by

$$\frac{x^2}{a^2}+\frac{y^2}{b^2}=1 \qquad (11)$$

where a and b are the major (E-W) and minor (N-S) axes of the ellipse.

Figure 20 illustrates the approach for computing the weight factor (or the correlation distance). The figure shows a large ellipse computed from Eq. (11). This is the boundary at which the weight factor 'q' is zero. The updating VI site is at the center of this ellipse. The grid point 'P' to be updated is at a distance r and at an azimuth θ measured from the X-axis, which is the major axis of the ellipse. The line from the center passing through P cuts the ellipse at the distance 'R'. At the center of the ellipse (that is, at the VI site) 'q' is 1 . If r is greater than R, the point is outside the boundary of the correlation ellipse, therefore q is set to zero (q=0). The value 'q' at the point P is given by the equation

$$q = 1 - \frac{r}{R} = 1 - r * \sqrt{\frac{\cos^2\theta}{a^2} + \frac{\sin^2\theta}{b^2}} \qquad (12)$$

In computing a distance and azimuthal location between two points on the earth the angle is measured with respect to north. For the ellipse (Figure 20), it is measured from the east with respect to the major axis. Therefore 90° should be subtracted from the azimuthal angle between the pair of the stations .

The axes of the ellipse 'a' and 'b' show seasonal dependence for both foF_2 and M(3000) parameters (Rush and Gibbs 1973). The quantities 'a' and 'b' are constant for a given season for a given parameter (foF_2, MUF).

Rush and Gibbs (1973) determined the weight factors for the geomagnetic (N-S and E-W) meridian reference frame. For this purpose the axes of the ellipse referred to in Eq. (12) have to be rotated so as to align the minor (b) axis along the geomagnetic N-S meridian. These angles are computed for each station and listed in the last column of Table 1. Taking into account a) the azimuthal difference between geographic and geomagnetic systems of coordinates, and b) the azimuthal angle for the ellipse with respect to east vs the azimuthal angle between stations with respect to north, the angle θ for Eq. (12) is computed by the equation

$$\theta = \theta_1 + \theta_2 - 90^\circ \qquad (12a)$$

where θ_1 is the angle from Table 1 for the VI site and θ_2 is azimuthal angle between the VI site and the grid point.

Updating with VI site data: To overcome the shortcomings of the current updating scheme (see Section 3.5, item 2 above) we propose to use all the sites for updating the model at a given grid point out to the maximum range of their respective correlation distances (R=0) with restrictions in items 2 and 4. Therefore we replace Eq. (90-52) by the equation

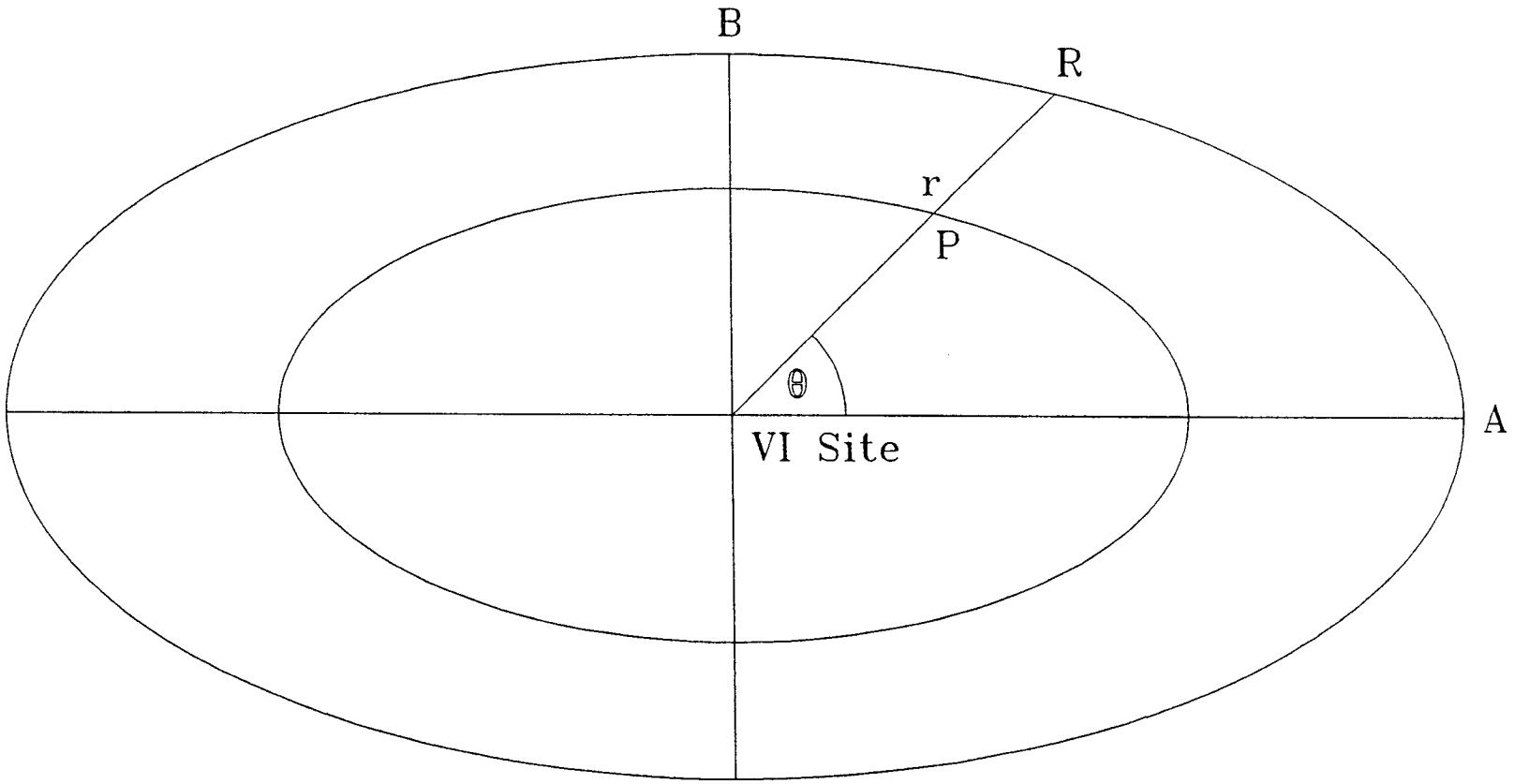

Figure 20. Illustration for Using Correlation Ellipse for Determination of a Weight Factor q.

$$x'_p \frac{\sum x_i * q_i}{\sum q_i} \tag{13}$$

where x_i is the percent difference between the observation and the prediction in the ionospheric model parameter at the i^{th} VI site, q_i is the distance dependent weight factor defined in Eq. (12) and the summation is done for all the VI sites from which the real time data are available for the time of updating the model. Note that the correlation coefficient/weight factor 'q_i' is the level of reliability/confidence in the covariation, but does not provide the magnitudes of the respective variations.

As discussed above, the updating scheme is proposed for all DISS and ECRS VI sounders in daytime, with limits after sunset, to prevent cross-talk from trough/oval stations into the midlatitude ionosphere and vice versa. The area of influence limits are as previously discussed, the Q_E/K-AWS driven trough and oval boundaries.

The seasonally dependent constants 'a' and 'b' in Eq. (12) are computed from the data in Table XLI pp.1876-1877 (Carl Bowser unpublished report). A straight line is fitted to each data set with the condition the line passes through (0,1.0), so that the correlation is 1.0 at the VI site where the separation distance is zero. The equation for this straight line is given by

$$y = mx+1. \tag{14}$$

Using the least squared deviation technique, we get the slope m from the equation

$$m = \frac{\sum y_n - n}{\sum x_n} \tag{15}$$

where the summation is done for all the 'n' non-zero (weight) data points.

The results for the straight line fit to the data in Table XLI (pp 1876-1877, Carl Bowser unpublished report) are presented in Table 4.

Table 4. Empirical Straight Line Fit of Weight Factors to Data in Table XLI (p. 1876-77 Carl Bowser unpublished report)

PARAMETER	SEASON / DIRECTION	NOV-FEB	MAR-APR SEPT-OCT	MAY-AUG
foF_2	E-W	–0.271	–0.122	–0.143
	N-S	–0.350	–0.203	–0.210
M(3000)	E-W	–0.308	–0.318	–0.460
	N-S	–0.580	–0.351	–0.713

The correlation coefficients and the straight line fit are shown in Figures 21-23 for the parameter foF_2 and in Figures 24-26 for M(3000). In each figure we have two sets of weight factors: a) along the N-S direction, and b) along the E-W direction. Note that each straight line passes through the point (0,1). The cutoff along the distance axis is the value for the constant 'a' for the E-W direction and 'b' for the N-S direction. The 'a' and 'b' are the major and minor axes of the ellipse in Eq. (12).

The equal weight contours for these data are computed using Eq. (12). These are shown in Figures 27-29 for foF_2 and in Figures 30-32 for M(3000). Note that the ellipse is largest for foF_2 for the Apr-May, and Sept-Oct periods and is smallest for M(3000) for the period May-Aug. One may compare the shape of curves in Figures 23-28 with that shown in Figure 18 determined from Eq. (90-41) on p.1878 (Carl Bowser, unpublished report).

In the computer one can now use three sets (for three seasons) of 'a' and 'b' values listed in Table 5 for each of the parameters foF_2 and M(3000) in place of the data in Table XLI on pp. 1876-77 (Carl Bowser, unpublished report).

Table 5. Major (a) and Minor (b) Axes (km) of Correlation Ellipse

PARAMETER	SEASON	a	b
foF_2	NOV-FEB	3690	2850
	MAR-APR SEPT-OCT	8180	4920
	MAY-AUG	7010	4770
M(3000)	NOV-FEB	3250	1720
	MAR-APR SEPT-OCT	3150	2850
	MAY-AUG	2170	1400

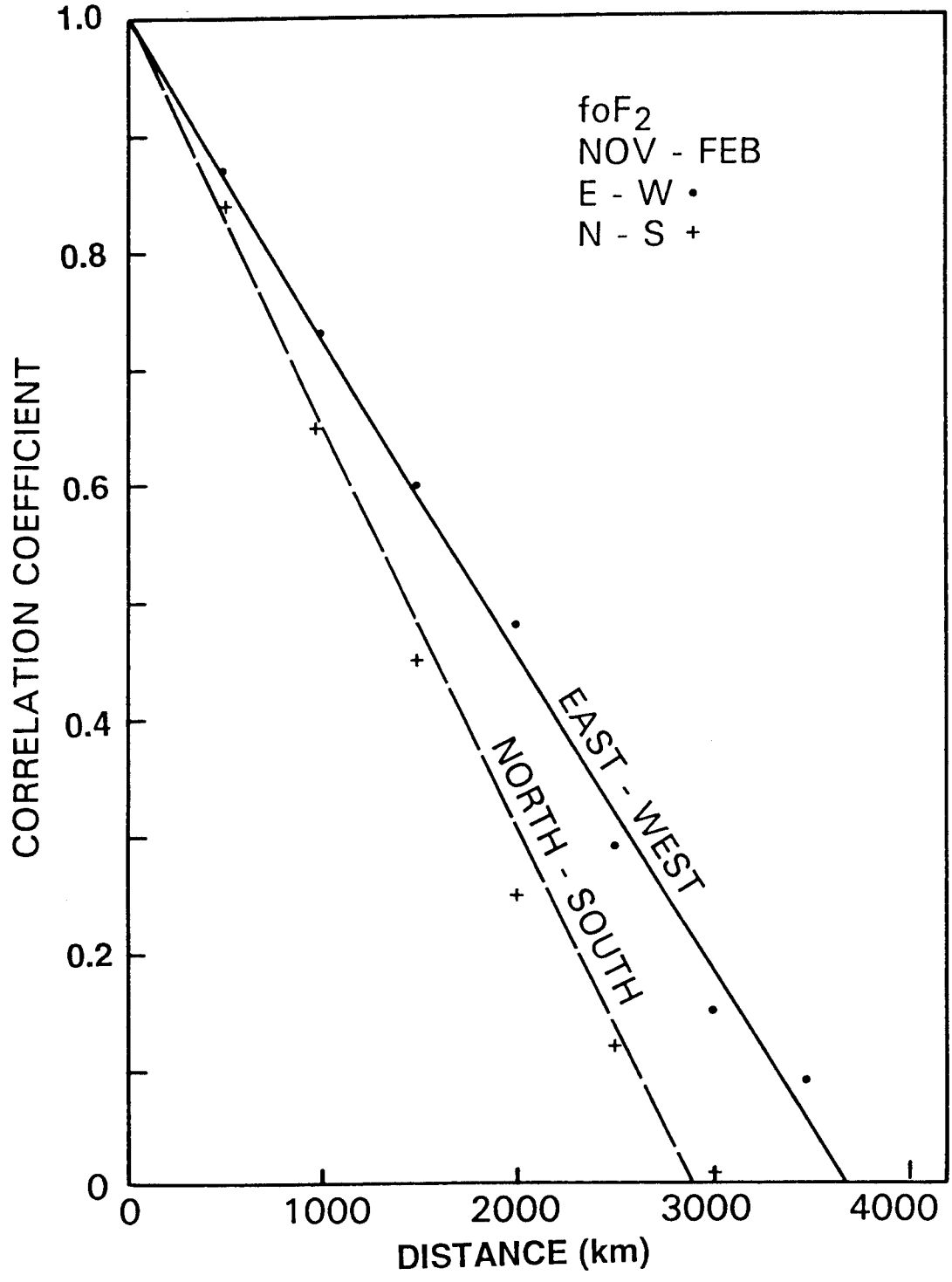

Figure 21. Dependence of the Correlation Coefficient (Weight Factor) on Separation Between VI Sites Along N-S and E-W Directions for foF_2 for November-February Period.

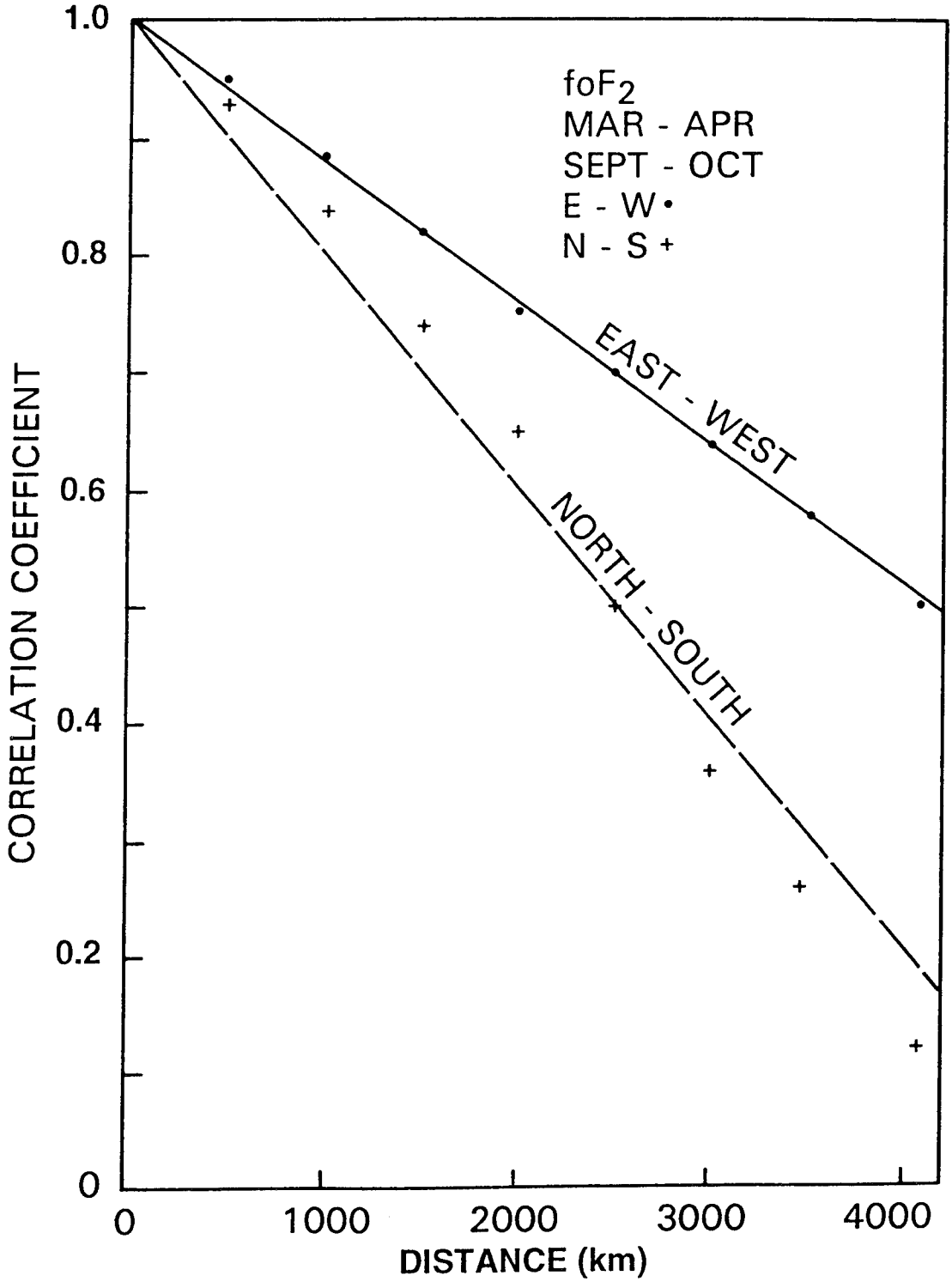

Figure 22. Dependence of the Correlation Coefficient (Weight Factor) on Separation Between VI Sites Along N-S and E-W Directions for foF_2 for March-April and September-October Period.

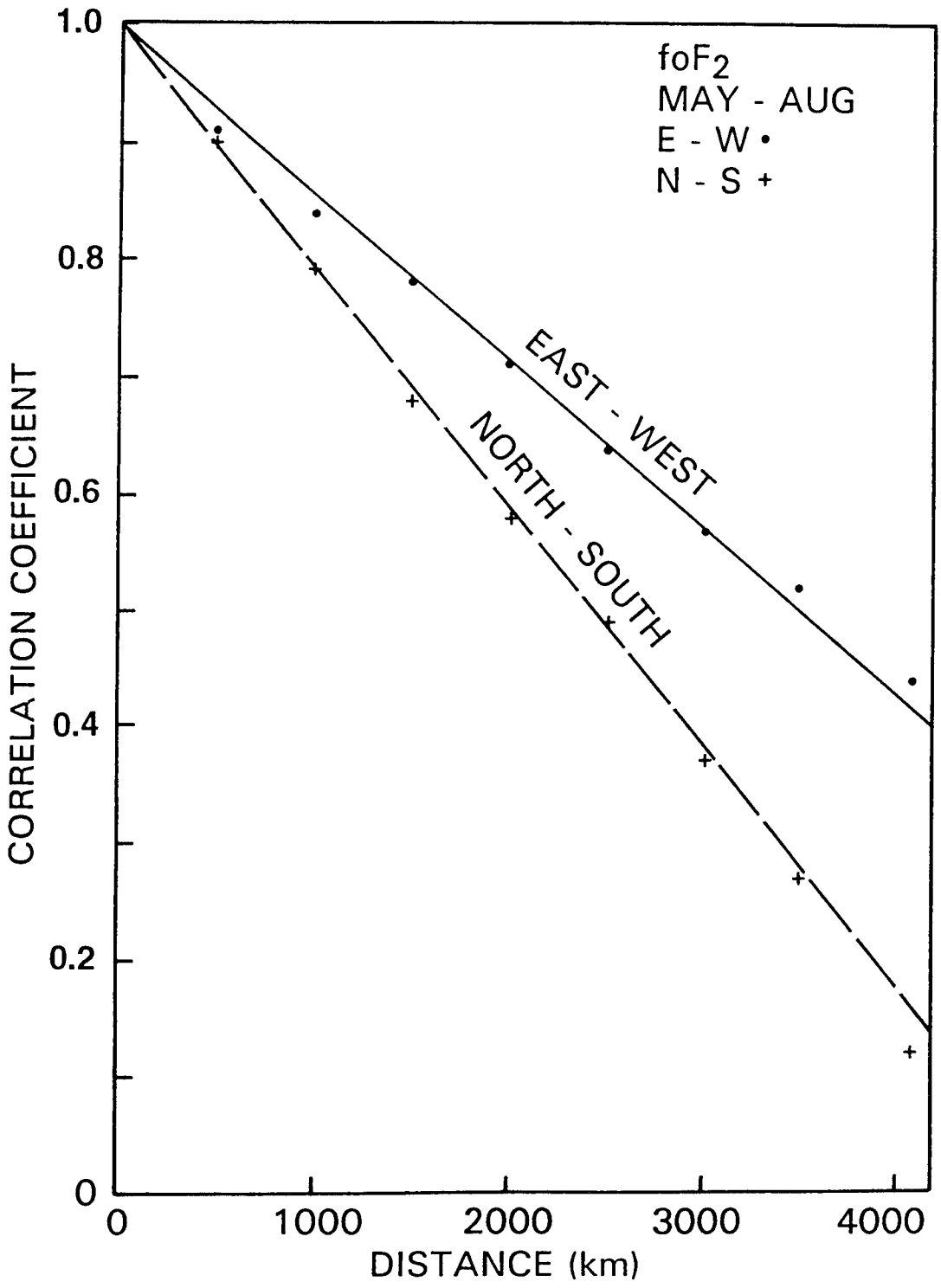

Figure 23. Dependence of the Correlation Coefficient (Weight Factor) on Separation Between VI Sites Along N-S and E-W Directions for foF_2 for May-August Period.

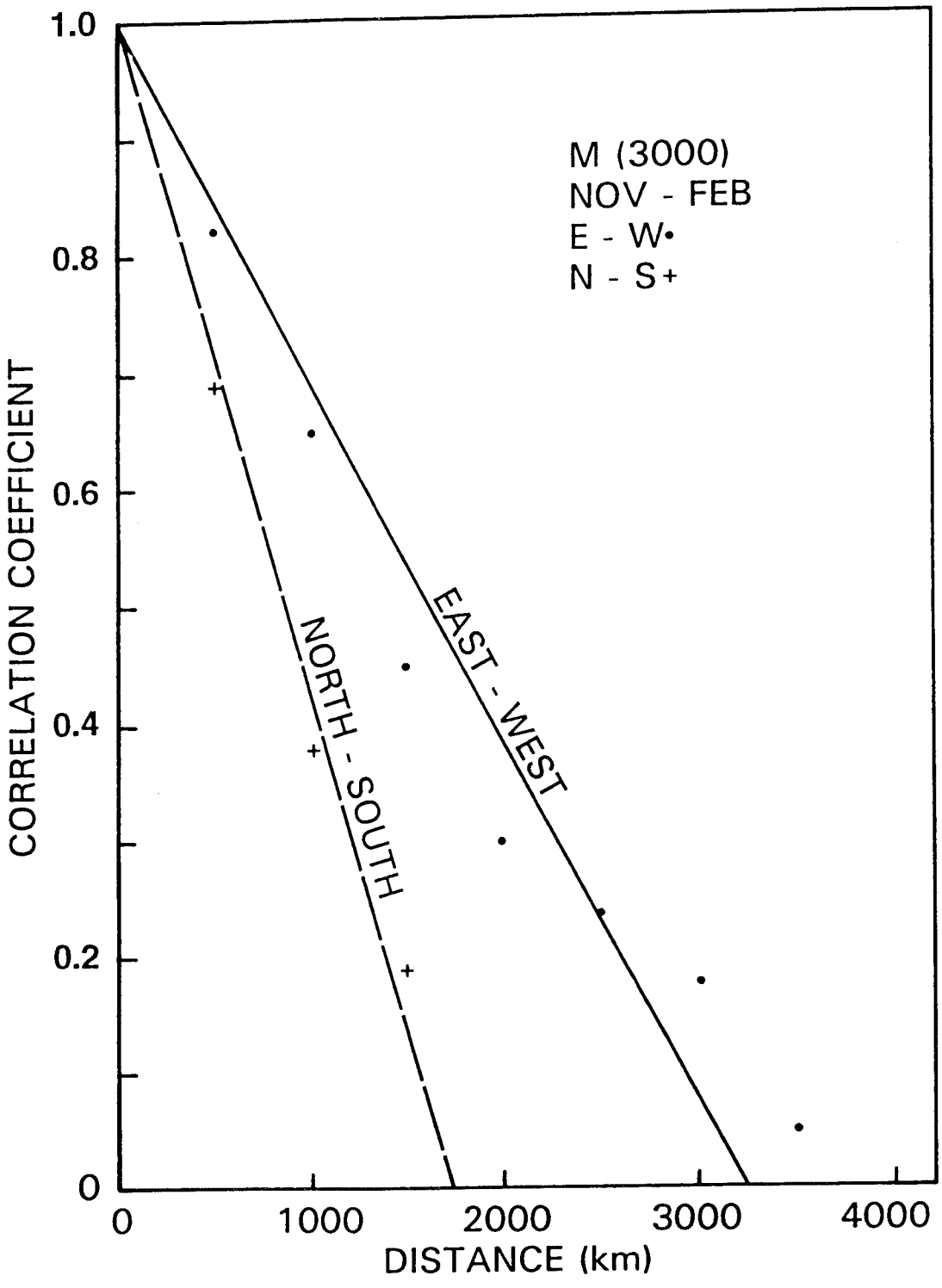

Figure 24. Dependence of the Correlation Coefficient (Weight Factor) on Separation Between VI Sites Along N-S and E-W Directions for M(3000) for November-February Period.

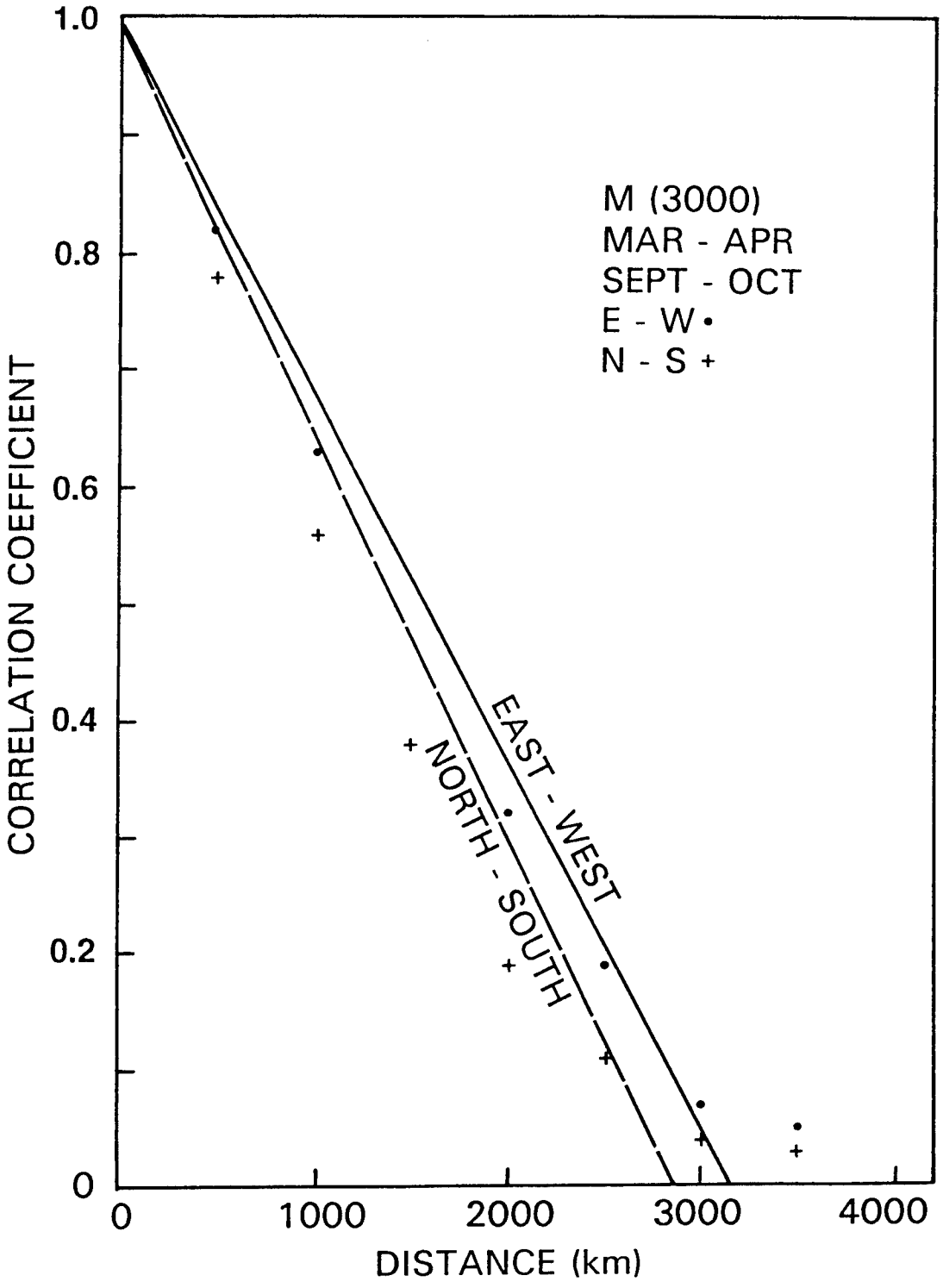

Figure 25. Dependence of the Correlation Coefficient (Weight Factor) on Separation Between VI Sites Along N-S and E-W Directions for M(3000) for March-April and September-October Period.

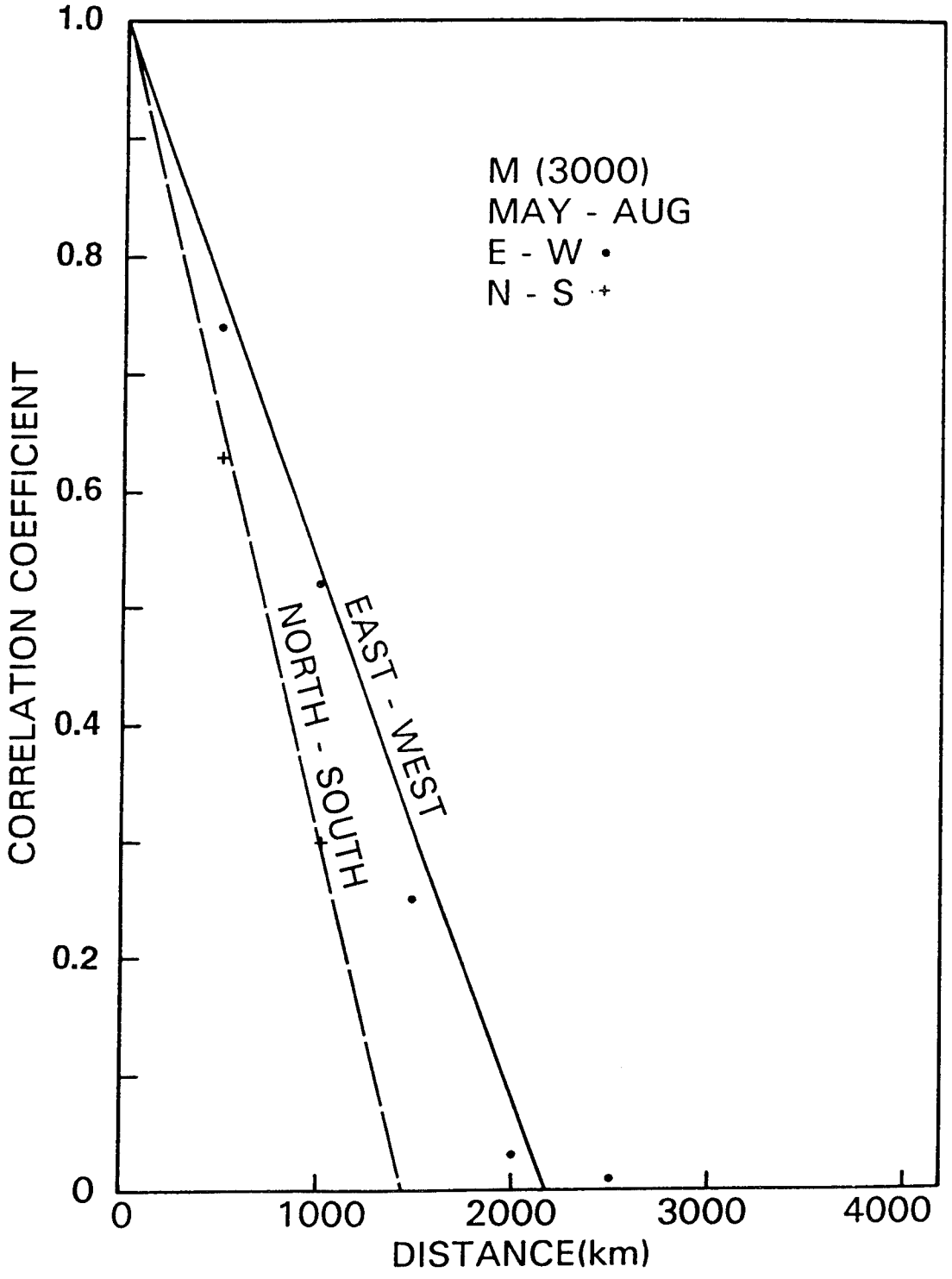

Figure 26. Dependence of the Correlation Coefficient (Weight Factor) on Separation Between VI Sites Along N-S and E-W Directions for M(3000) for May-August Period.

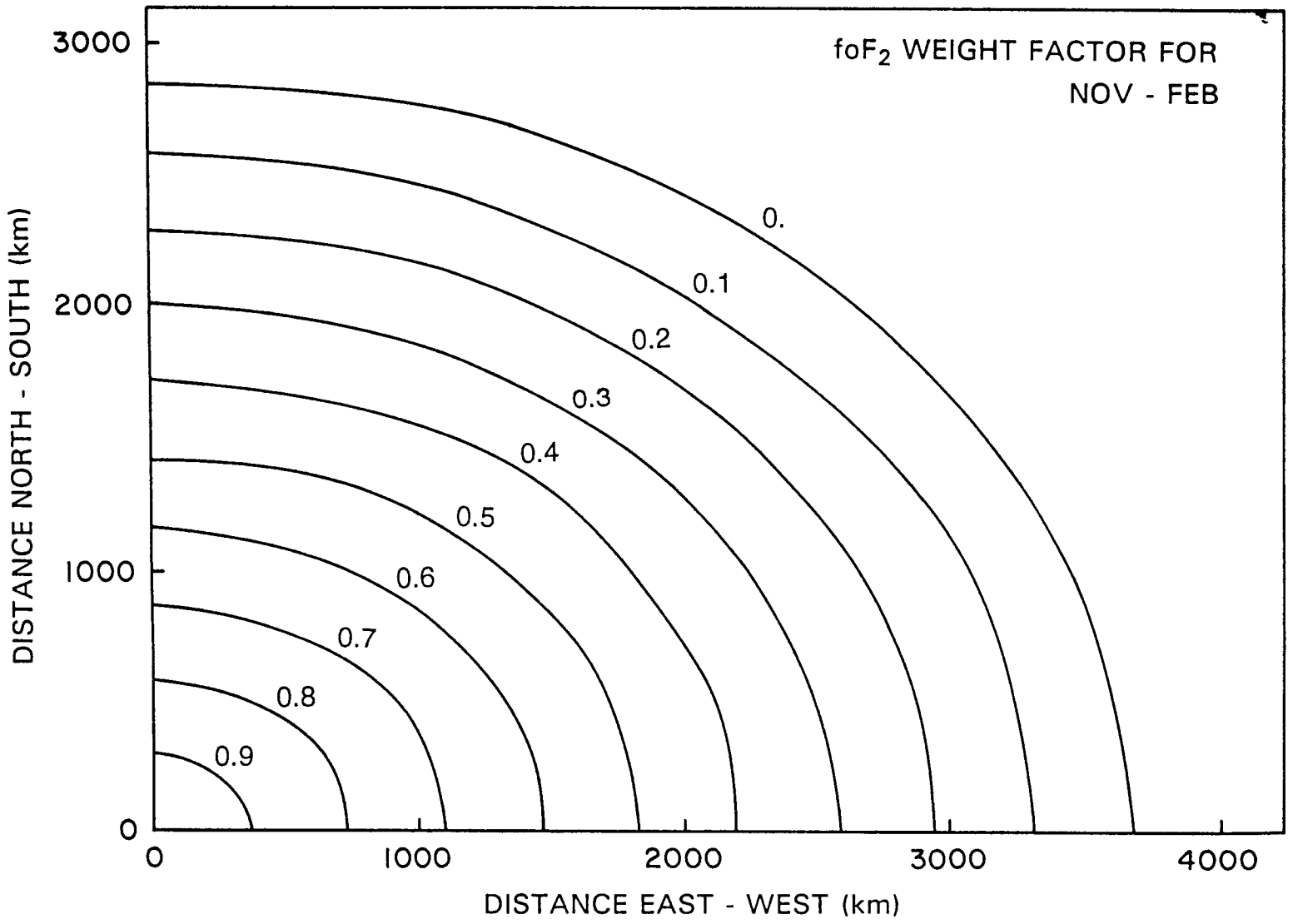

Figure 27. Weight Factor Contours for foF_2 for November-February Period.

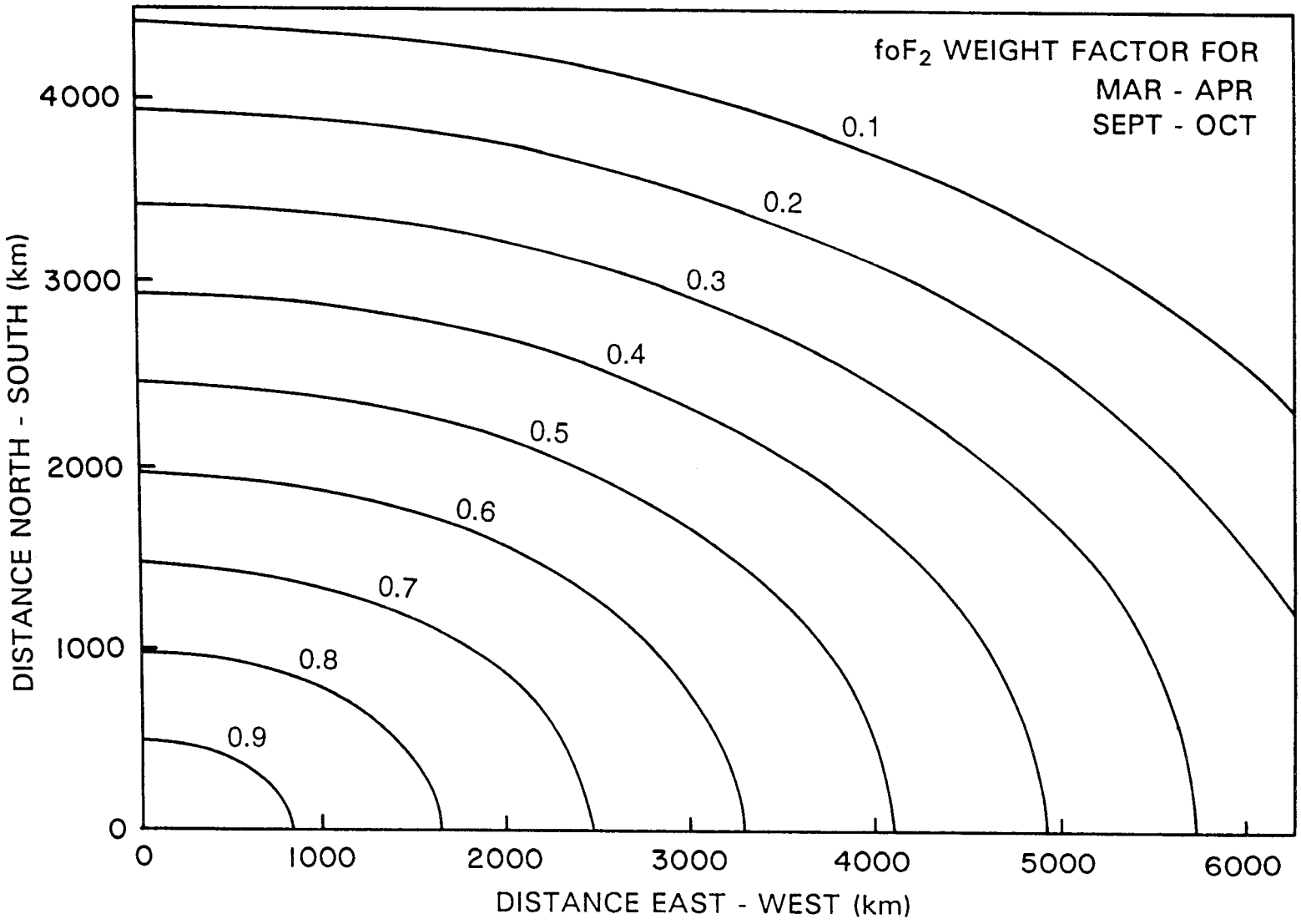

Figure 28. Weight Factor Contours for foF_2 for March-April and September-October Period.

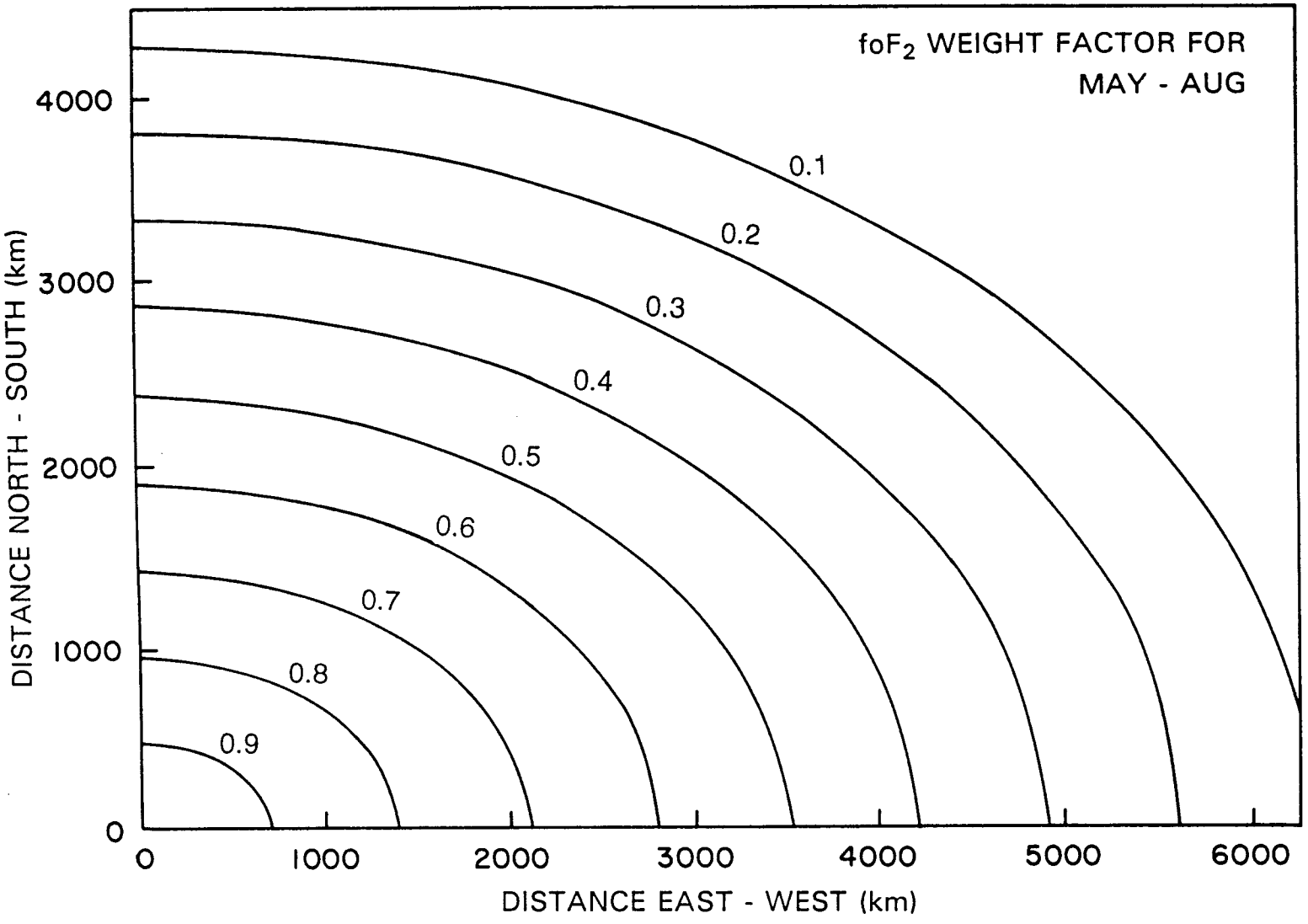

Figure 29. Weight Factor Contours for foF_2 for May-August Period.

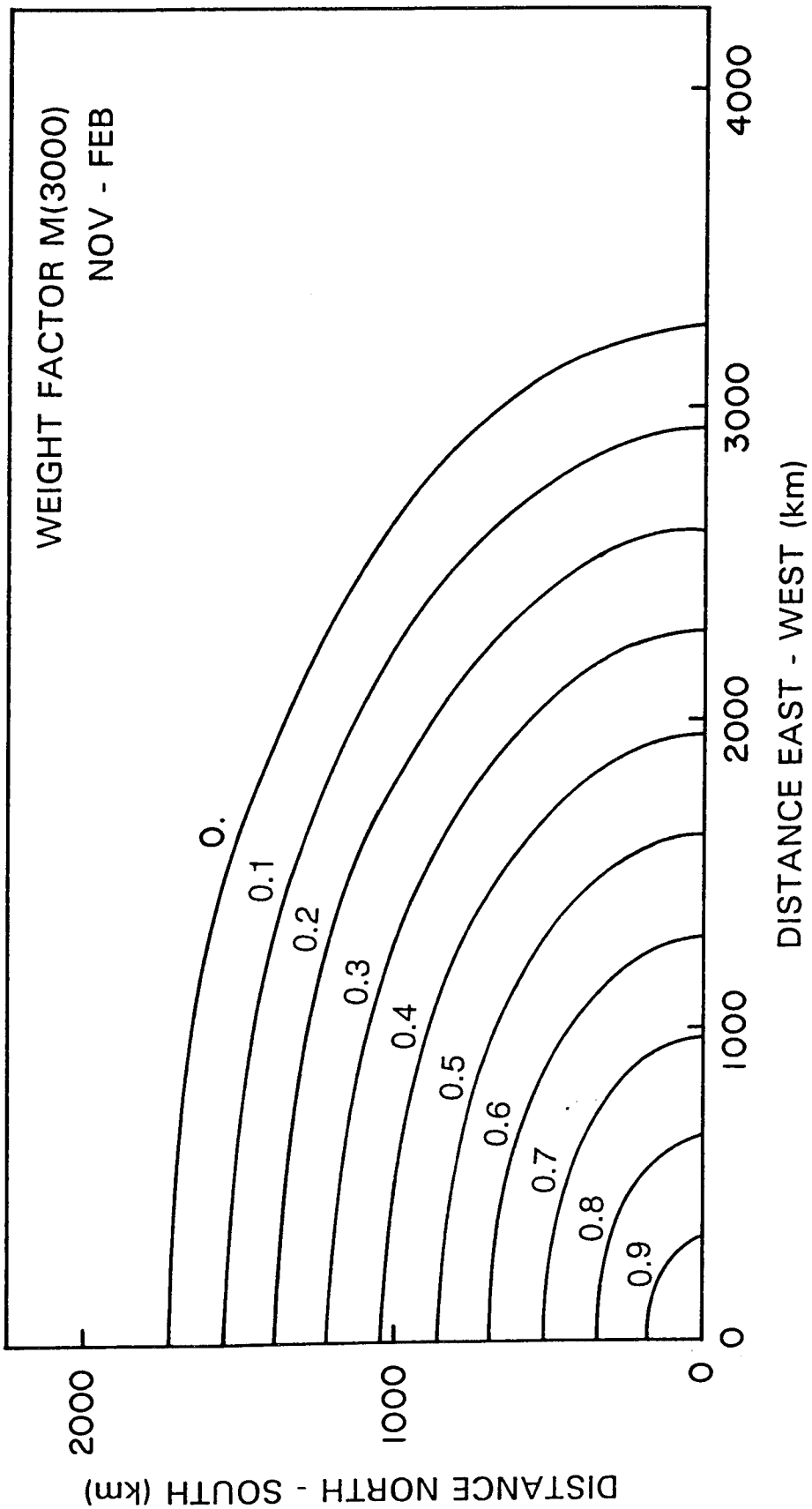

Figure 30. Weight Factor Contours for M(3000) for November-February Period.

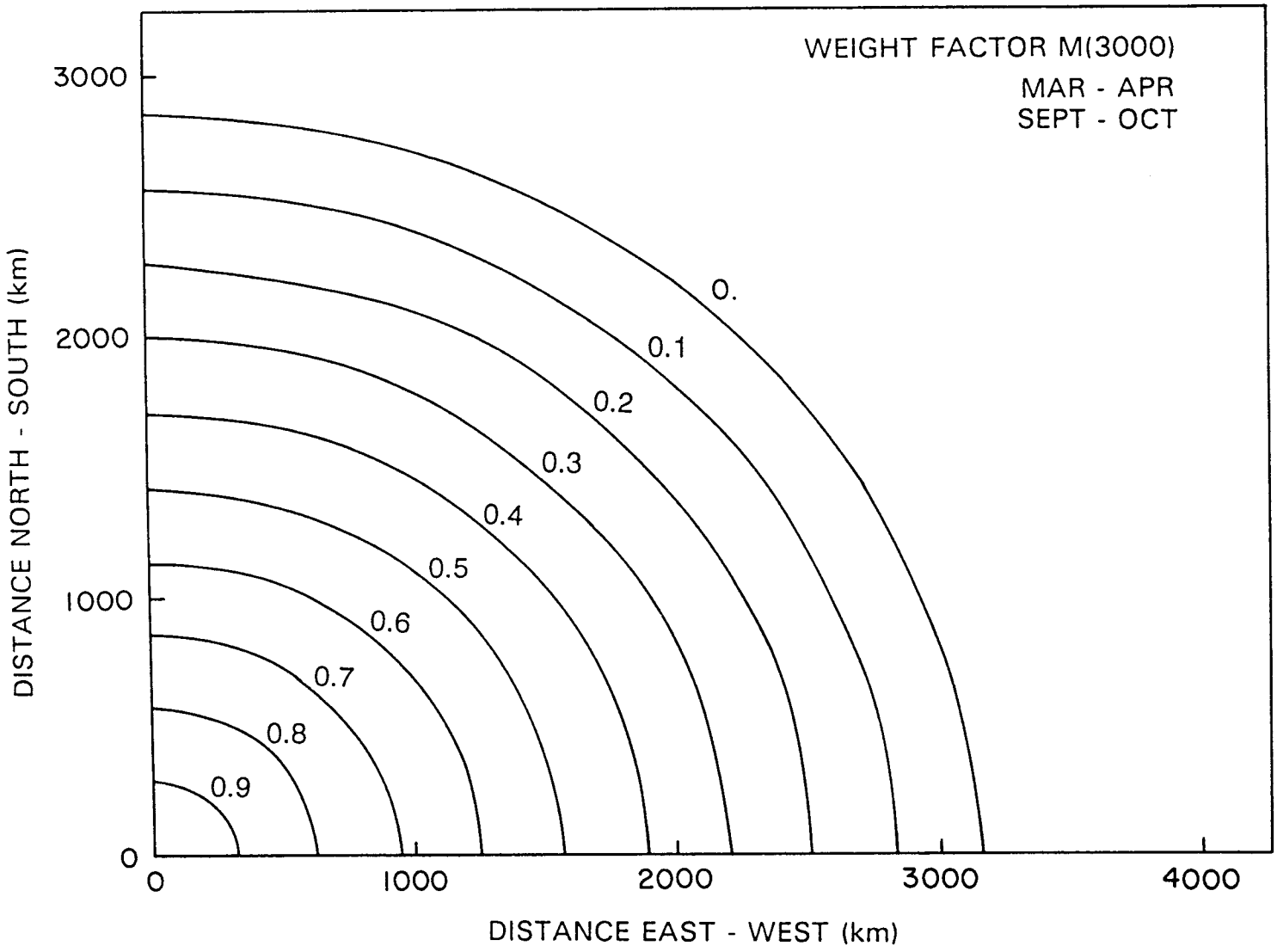

Figure 31. Weight Factor Contours for M(3000) for March-April and September-October Period.

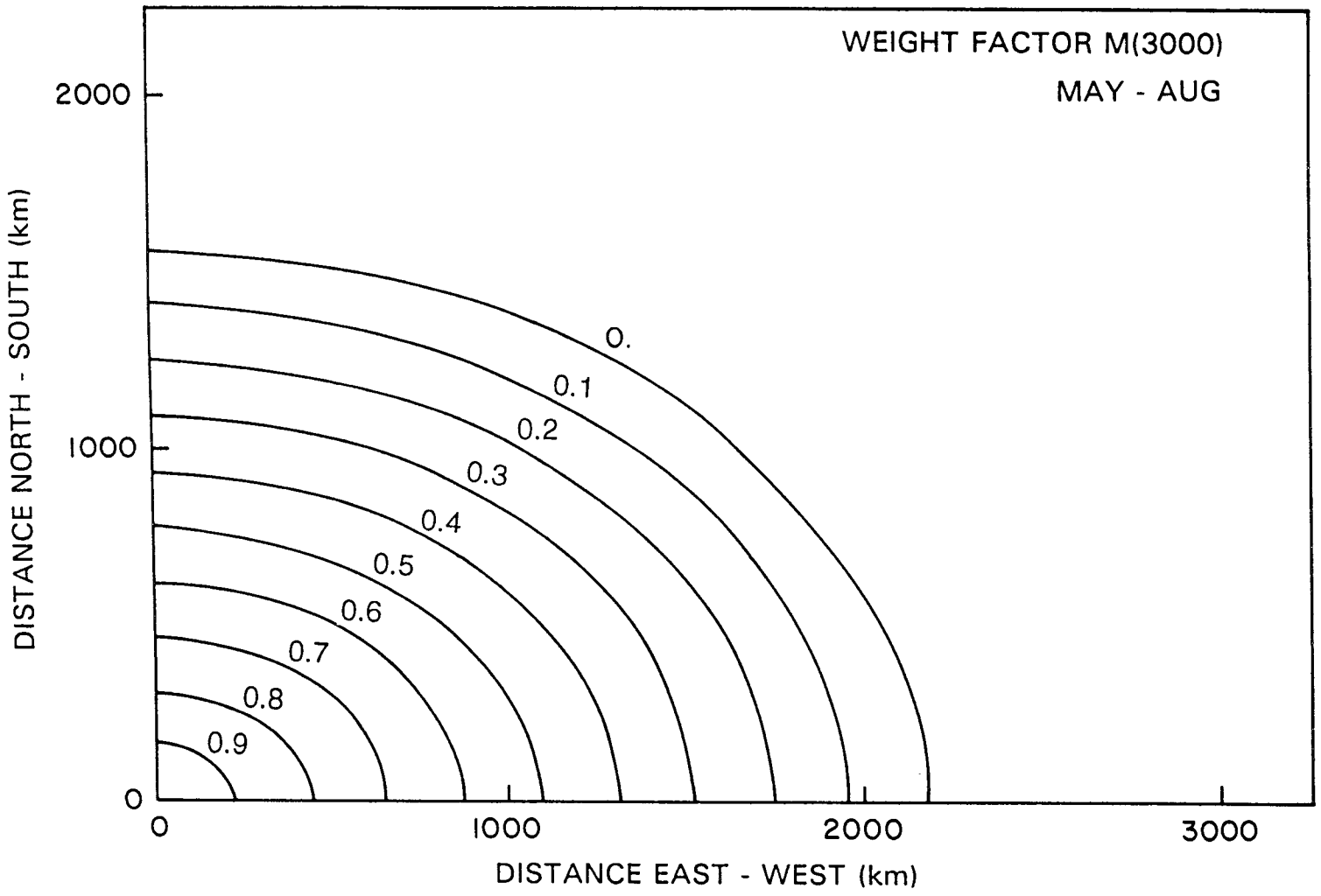

Figure 32. Weight Factor Contours for M(3000) for May-August Period.

The distance x and y of the grid point from the VI sites is computed using the geographic system of coordinates (not geomagnetic coordinates as done in the GE approach) and the ellipse is aligned along the magnetic meridian using the values of the angle 'θ' between the geomagnetic and geographic meridian at the VI site listed in Table 1.

5. CONCLUSIONS

This preliminary report summarizes the results of two tests of the OTH model installed at the PL facility. Several inaccuracies in the concept and formulation of the auroral E layer, F layer trough and the updating scheme using real time VI-site data have been summarized. A way to correct the respective inaccuracies has been discussed. In the near future we plan to complete these modifications and test the 'improved' model with additional data collected during the OTH radar DT&E campaign conducted in October 1989.

6. MISCELLANEOUS CORRECTIONS AND COMMENTS

As the GE document (Carl Bowser unpublished report) is an indispensable source for the procedure for coordinate registration and the ionospheric modeling used at the OTH radars, additional typographical and other errors and comments are listed below. For convenience and simplification these are listed in sequential order.

pp.1863 B, C, and D: The equations use a term 600 in the denominator. This term should be the denominator only for the negative term in the bracket. The computer program of the corresponding part is written properly with no error.

p.1863 E line 5: should read mult=W__ccc_VI1-GP*mult; on line 3 from the bottom 2VI should read VI2.

p.1863 E,F: There are two F_2 layer adjustment schemes; one listed here and the other on pp.1878-80. The scheme listed here is proper and better than the one on pp.1878-80.

p.1865: in Eq. (90-3f) the first negative (-) sign on the R.H.S. should be replaced by a positive (+) sign.

p.1870: in Eq. (90-23) the positive sign (+) in the [] bracket should be replaced by a negative (-) sign.

p.1873: in Eq. (90-35) $[B_E\text{-}4A_EC_E]^{1/2}$ should read $-[B_E{}^2\text{-}4A_EC_E]^{1/2}$.

p.1876: col 3, line 8, Table for E-W direction, .09 should read .07.

p.1876: bottom line columns 4 and 5 should read .14 and .17 respectively.

p.1877: column 3, lines 6,7,8, Table of E-W direction should read .18, .05, and .02 respectively.

p.1877: last column, no. 5, Table for N-S direction line 4 should read .15.

p.1880: Eq. (90-52) The denominator 2 is needed if both K_1 and K_2 are non-zero. If either is zero the real value of x_p would be divided by 2.

p.1884: lines 7-8, one needs vertical height estimates from a vertical incidence sounder in the vicinity where the reflections of the radar and/or target signal takes place, not in the vicinity of the radar or the target.

p.1961: lines 22-23. This condition of removing F1 layer when $foF_1 > foF_2$ results in discarding the low altitude F_1 layer ionization. The F_1 layer is allowed to build up to the time it becomes equal to or stronger than foF_2. In effect we are throwing away the stronger low altitude ionization.

p.1966 In Eq. (190-41) ϕ_A should read ϕ_E.

p.1967: In Eqs. (190-49) and (190-50) the equations should have a negative (-) sign following the equal to (=) sign.

p.1967: On line 15 the equation numbers (190-4) and (190-6) quoted refer to the E layer and not to the F_2 layer under discussion.

p.1968: On line 10 the Eq. (190-4) refers to the E layer and not to the F_2 layer under discussion.

References

1. Millman, G.H., Bowser, C.A. and Swanson, R.W. (1988) An ionospheric model for HF sky wave backscatter radar, NATO-AGARD Symposium on Ionospheric Structure and Variability on A Global Scale and Interactions with Atmosphere, Magnetosphere, Munich, Federal Republic of Germany, *AGARD Conf. Proc.* **441**:pp. 43-1 to 43-15.

2. Air Force Global Weather Central (1982) *AFGWC Polar Ionospheric Model*, Air Force Global Weather Central, Program Listing.

3. Jones, W.B., Graham, R.P. and Leftin, M. (1969) *Advances in Ionospheric Mapping by Numerical Methods*, National Bureau of Standards U. S. Dept. of Commerce NBS Tech. Note 337, May (Reissued as ESSA Tech. Note ERL 107 ITS 75 May 1969).

4. Bowser, C., *AN/FPS 118 Analytical Model Specification, Preliminary Draft*, Contractor General Electric Company, private communication.

5. Feldstein, Y.I. and Starkov, G.V. (1967) Dynamics of auroral belt and polar magnetic disturbances, *Planet. Space Sci.* **15**:209-229.

6. Wagner, R.A. (1972) Modeling the Auroral E-layer in Arctic Ionospheric Modeling. Five related papers by Gassman, G.E., Buchau, J., Wagner, R.A., Pike, C.A. and Hurwitz, M.G., *Air Force Surveys in Geophysics*, No. 241, AFCRL-72-0305, AD748796.

7. Whalen, J.A. (1983) A quantitative description of the spatial distribution and dynamics of the energy flux in the continuous aurora, *J. Geophys. Res.*, **88A9**:7155-69.

8. Whalen, J.A. O'Neil, R.R. and Picard, R.H. (1985) The Aurora, in *Handbook of Geophysics and the Space Environment*, Air Force Geophysics Laboratory, AFGL-TR-85-0315, ADA16700.

9. Starkov, G.V. (1969) Analytical representation of the equatorial boundary of the auroral oval zone, *Geomag. and Aeronomy (Eng. Ed)*, **9**:614.

10. Whalen, J.A. (1987) The daytime F layer trough observed on a macroscopic scale, *J. Geophys. Res.*, **92**:2571.

11. Whalen, J.A. (1989) The daytime F layer trough and its relation to ionospheric – magnetospheric convection, *J. Geophys. Res.*, **94**:17169.

12. Halcrow, B.W. and Nisbet, J.S. (1977) A model of F_2 peak electron densities in the main trough region of the ionosphere, *Radio Science*, **12**:815-820.

13. Dandekar, B.S. The statistical relations among Q, Kp and the Global Weather Central K-indices, *Environmental Research Papers*, No. 763, AFGL-TR-82-0010, ADA118734.

14. Gussenhoven, M.S., Hardy, D.A. and Heinemann, N. (1983) Systematics of the equatorward diffuse auroral boundary, *J. Geophys. Res.*, **88**:5692.

15. Rush, C.M. and Gibbs (1973) Predicting the day-to-day variability of the mid-latitude ionosphere for applications to HF propagation predictions, *Air Force Surveys in Geophysics No. 268*, May, AFCRL-TR-73-0335, AD764711.

16. Barghausen, A.F., Finney, J.W., Proctor, L.W. and Schultz, L.D. (1969) Predicting long-term operational parameters of high frequency sky wave telecommunication systems, *ESSA Technical Report ERL 110-ITS-78*, Washington, DC.

17. Gautier, T.N. and Zacharisen, D.H. (1965) *Use of Space and Time Correlation in Short-term Ionospheric Predictions*, First Annual IEEE Communications Convention, Boulder, Colorado, June 7-9, pp. 671-676.